Utrecht University

IMAU, Institute for Marine and Atmospheric Researh

KNMI, Royal Dutch Meteorological Institute

Master Thesis

The value of aircraft data in investigating the cause of a severe storm

Author:
Patrick Van den Hoek
5498325
Master Meteorology, physical oceanography and Climate

Supervisors:
Dr. Aarnout Van Delden
Dr. Siebren De Haan

August 9, 2016

Abstract

The storm of the 28 of October 2013 was one of the strongest of the last 10 years, with wind gusts up to 152 km/h above the Wadden islands. In Meteorologica, a discussion started about the cause of the high winds experienced during this storm. With the help of Mode-S EHS aircraft data it is investigated to what extent the isallobaric wind has a large contribution to the total wind field. Mode-S EHS data, which is accumulated from an enhanced surveillance air traffic control radar that follows all the aircrafts in its range, contains information about the wind and the temperature. The quality of Mode-S EHS data is checked by a comparison with the Cabauw tower and the wind profiler at Cabauw. From this comparison, it is found that the quality of the Mode-S EHS data is good to use for further research. For the case study of the storm of the 28 of October 2013, the theoretical wind is determined with the finite difference method and with the piecewise linear interpolation method with the geopotential height from Harmonie 38h1.2. With these two methods the geostrophic wind, the isallobaric wind and the inertial-advective component of the ageostrophic wind are determined. From this, it follows that the isallobaric wind and the inertial-advective component of the ageostrophic wind counteract each other near the center of the extratropical cyclone. It also shows that the modelled wind from Harmonie 38 compares well with the wind speed measured by Mode-S EHS and that the high winds were manifested in the lowest 800 m of the atmosphere.

Contents

Chapter 1

Introduction

A discussion started in the Dutch magazine Meteorologica about the cause of the high wind speeds during the storm of the 28 of October 2013. This storm is in the top ten most severe storms of the Netherlands. The record wind gust measured for the month October over the Netherlands was measured on this day. Van Delden (2013) stated that the large wind speeds were caused by the isallobaric effect. The isallobaric wind blows from pressure rises to pressure falls and has a large contribution in fast moving and fast developing cyclones. De Bruin (2014) stated that the isallobaric wind is not enough to only describe the strong winds, but also the other components of the ageostrophic wind should be taken into account. One of these components is the inertial advective component of the ageostrophic wind, blowing in the southern region of a trough, in the opposite direction of the geostrophic wind. The outcome of the discussion is still open, and therefore interesting to investigate [12].

A Mode-S EHS (Mode-Secondary Enhanced Surveillance) radar is used to detect all aircrafts in its range, where the air traffic control uses this radar to determine the position and the intention of the aircraft. It is found that from this data the wind and temperature can de derived, where this research was set-up to use the Mode-S EHS measurements in a case study. The Mode-S EHS data is used to investigate the role of the isallobaric wind.

This master thesis describes the Mode-S EHS data and the case study of the storm of the 28 of October 2013. The main research question is,

Is the isallobaric wind the source of the high wind speeds measured above the Netherlands during the storm of the 28 of October 2013?

This thesis is devided into three chapters. The first chapter explains the theory, containing information about the set-up of the Mode-S EHS data, an introduction in the ageostrophic wind and the theory of the wind profiler used in the comparison. The second chapter describes the validation of the quality of the Mode-S EHS data, determined by comparing the Mode-S EHS with the Cabauw tower and a wind profiler. The third chapter focuses on the case study of the storm of 28 October 2013, where the wind is derived from the theory of Chapter 1 and compared with the Mode-S EHS and Harmonie 38, the weather model of the KNMI.

Chapter 2

Theory

The Mode-S EHS data is used to determine the wind speed over a wide range of heights in the atmosphere. This chapter describes the theory behind the Mode-S EHS, the theory of the ageostrophic wind and the theory behind the wind profiler. First it is explained how the wind is determined from the Mode-S EHS and which corrections are made to use the data. The second part describes the flow in the atmosphere, with particular attention payed to the components of the ageostrophic wind. The third part describes the theory behind the wind profiler, which is used in the comparison with the Mode-S EHS data.

2.1 Mode-S EHS

Aircrafts can be used to measure the atmospheric wind profile in the vicinity of airports and can be equipped with AMDAR (Aircraft meteorological Data Relay) to measure meteorological data during their flight, but not all aircrafts are equipped with this software. An enhanced tracking and ranging by an EHS (EnHanced Surveillance) air traffic control radar follows all the aircrafts in its measurement range. The Mode-S EHS radar is used by the air traffic control to determine the location and the intention of the aircrafts. The TAR-radar at Schiphol has a range of 270 km and is capable to receive Mode-S (Mode secondary) EHS transponder information. Every four seconds the radar contacts each aircraft on which the transponder responds with a data-message [3].

The Mode-S EHS data contains information on: flight level (F), Mach number (m), roll, true airspeed (V_t), heading (α_t), ground speed (V_{gr}) and track angle (α_{gr}). From this data, the wind speed, wind direction and temperature can be derived. The Mach number is the ratio between the true airspeed and the speed of sound, where the true air speed is the speed of the aircraft relative to the airmass in which it is flying. The Mach number is calculated by the board computers in the aircraft from the measured temperature and the true air speed. From the Mach number, the temperature can be written as [2],

$$T = \frac{1}{\gamma R_d} \frac{V_t^2}{m^2}, \tag{2.1}$$

where T is in K, $\gamma = c_p/c_v$ is the ratio of specific heats, R_d is the gas constant of dry air ($R_d = 287$ Jkg^{-1}K^{-1}). The aircraft measures the speed of the aircraft relative to the airspeed, where the ground track of the aircraft can be determined by the change in the position of the aircraft. With the use of the ground speed and the true air speed of the aircraft, the wind vector can be calculated, which is defined as the sum of the true air speed vector plus the ground speed vector. So the wind vector can be written as,

$$\vec{V} = \vec{V_{gr}} - \vec{V_t}, \tag{2.2}$$

where $\vec{V}$ is the wind vector in ms^{-1}, $\vec{V_{gr}}$ is the ground track vector and $\vec{V_t}$ is the true airspeed vector. The sum of the two vectors is also illustrated in figure 2.1, showing in blue the true air speed vector, in red the ground speed vector and in black the wind vector.

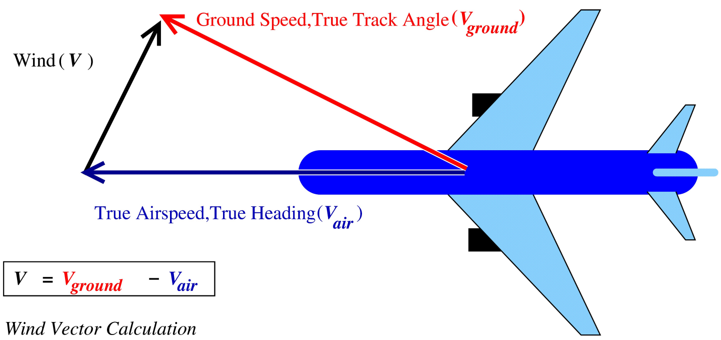

Figure 2.1: The true airspeed vector (blue) and the ground speed vector (red), where the sum defines the wind vector (black).

Some corrections are made to make the sum of the vectors useful to determine the wind speed. A correction in the magnetic heading of the aircraft is done to correct for the difference between the true North Pole and the magnetic North Pole, which is automatically done by the systems of the aircrafts. The magnetic pole moves from position in time, but the position of the magnetic pole, known by the aircrafts, is updated every ten year, so a correction is needed to correct for this difference in the position of the true North Pole and the magnetic North Pole [1].

The true air speed is measured by the aircraft with the use of pitot probes, which measure the wind speed from the pressure, and consists of a tube which is directed in the flow direction which is mounted on the body of an aircraft. The air flows into the tube with no outlet flow, so is brought in stagnation. The measured pressure in the tube is known as the stagnation pressure, which is defined as the sum of the static pressure plus the dynamic pressure following the law of Bernoulli [1]. Since the flow around an aircraft changes during different flight phases the Federal Aviation Administration prescribes the correction in the wind speed this is done by the use of the wind speed measured by the KNMI Doppler weather radar and ECMWF.

When the aircraft has a roll angle to the left or the right direction, the wind measurements are removed from the Mode-S EHS data, this is done due to the increase in the uncertainty in the calculation of the wind speed. Figure 2.2 illustrates the two corrections in the heading and the wind speed. The dashed lines show the uncorrected vectors and the thick lines show the corrected vectors.

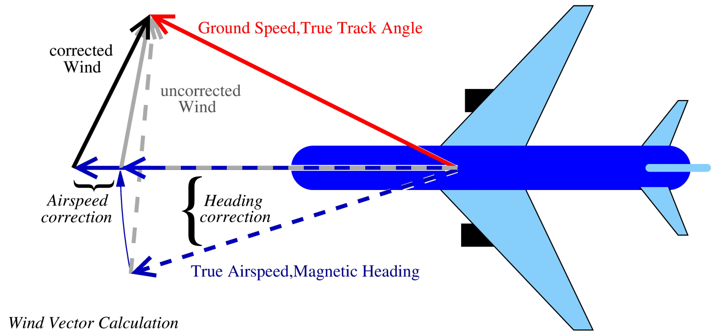

Figure 2.2: The corrected true airspeed vector (red) and ground speed vector(blue), which define the corrected wind vector (black).

2.2 The ageostrophic wind

The flow in the atmosphere above the boundary layer is roughly in geostrophic balance, which means that the pressure gradient force is in balance with the Coriolis force. The geostrophic wind always blows parallel to the isobars with lower pressure to the left of the flow in the Northern hemisphere. The wind in the atmosphere can be divided into a geostrophic part and a ageostrophic part. The ageostrophic wind has a large component in the total wind vector when the flow is strongly curved and when pressure changes rapidly in time. For this reason it is of great interest for this research to look into the theory of the ageostrophic wind.

The flow on a sphere is described by the Euler horizontal momentum equations, which can be written in isobaric coordinates as,

$$\frac{\mathrm{d}u}{\mathrm{d}t} - \frac{uv\tan\phi}{a} + \frac{uw}{a} = -g\left(\frac{\partial z}{\partial x}\right)_p + fv + F_{rx} - 2\Omega w\cos\phi \tag{2.3}$$

$$\frac{\mathrm{d}v}{\mathrm{d}t} + \frac{u^2\tan\phi}{a} + \frac{vw}{a} = -g\left(\frac{\partial z}{\partial y}\right)_p - fu + F_{ry}, \tag{2.4}$$

A B C D E F G

where u, v and w are the wind components in the x- (longitude), y- (latitude) and z- (vertical) direction, ϕ is the latitude in degrees, a is the radius of the earth in m, g is the gravitational acceleration ($g = 9.81\,\mathrm{ms}^{-2}$), f is the Coriolis parameter ($f = 2\Omega\sin\phi$ in s^{-1}, Ω is the angular velocity of the earth ($\Omega = 7.292\cdot 10^{-5}\,\mathrm{s}^{-1}$) and F_{rx} and F_{ry} are the horizontal frictional forces. Subscript p shows that the gradient in the height is defined on surfaces of equal pressure. The different terms of the equations are described in table 2.1, which also gives the scale of the different terms.

The total derivative $\frac{\mathrm{d}}{\mathrm{d}t}$ in the horizontal momentum equations is defined as,

$$\frac{\mathrm{d}}{\mathrm{d}t} = \frac{\partial}{\partial t} + u\left(\frac{\partial}{\partial x}\right)_p + v\left(\frac{\partial}{\partial y}\right)_p + \frac{\mathrm{d}p}{\mathrm{d}t}\frac{\partial}{\partial p}. \tag{2.5}$$

For motions on mid-latitude synoptic scales the curvature terms in the equations of motion are not important. From table 2.1 it follows that in this conditions, the Coriolis force and the pressure gradient force are in balance with each other, this balance is defined as the geostrophic wind balance, written as,

Table 2.1: The description of the terms in equations 2.3 and 2.4 and the scale of the terms at mid-latitudes

Part	Describtion	Scale (ms^{-2})
A	Local acceleration and advective terms of the wind	10^{-4}
B	Curvature term	10^{-5}
C	Curvature term	10^{-8}
D	Pressure gradient force	10^{-3}
E	Horizontal component of the Coriolis force	10^{-3}
F	Frictional force	10^{-12}
G	Vertical component of the Coriolis force	10^{-6}

$$v_g = \frac{g}{f}\left(\frac{\partial z}{\partial x}\right)_p \tag{2.6}$$

$$u_g = -\frac{g}{f}\left(\frac{\partial z}{\partial y}\right)_p, \tag{2.7}$$

where u_g and v_g are the horizontal components of the geostrophic wind in the x and y direction. The total wind vector $\vec{V}$ is divided into a geostrophic and an ageostrophic part, which is written as,

$$\vec{V} = \vec{V_g} + \vec{V_a}, \tag{2.8}$$

where the ageostrophic wind is defined as the difference between the geostrophic wind and the measured wind. The pressure gradient force lets an air parcel accelerate from higher to lower pressure. The magnitude of the pressure gradient determines the speed of the geostrophic wind and the the Coriolis force deflects the moving air to the right on the northern hemisphere. The geostrophic approximation holds only for straight isobars but with curvature in the isobars, the centripetal force needs to be taken into account. The ageostrophic wind also describes the curvature of the isobars. To determine the ageostrophic wind, geostrophic wind balance is written in vector form, which becomes,

$$\vec{V_g} = \frac{g\hat{k}}{f} \times \nabla_p z, \tag{2.9}$$

where $\hat{k}$ is the unit vector in the vertical direction. The equations of motion in a situation with straight isobars can be written as,

$$\frac{\mathrm{d}u}{\mathrm{d}t} = fv - g\frac{\partial z}{\partial x} \tag{2.10}$$

$$\frac{\mathrm{d}v}{\mathrm{d}t} = -fu - g\frac{\partial z}{\partial y}. \tag{2.11}$$

With the geostrophic wind approximation and equation 2.8 these equations become,

$$\frac{\mathrm{d}u}{\mathrm{d}t} = f v_a \tag{2.12}$$
$$\frac{\mathrm{d}v}{\mathrm{d}t} = -f u_a. \tag{2.13}$$

The vector notation of these equations can be written as,

$$\vec{V}_a = \frac{\hat{k}}{f} \times \frac{\mathrm{d}\vec{V}}{\mathrm{d}t}. \tag{2.14}$$

The right hand side of equation 2.14 shows the change in time of the real wind, which can be expanded in its local tendency and advective parts. For synoptic scale flow the tendency in the geostrophic wind can be assumed larger than the tendency in the ageostrophic wind, so the ageostrophic wind can be written as,

$$\vec{V}_a = \frac{\hat{k}}{f} \times \left(\frac{\partial \vec{V}_g}{\partial t} + (\vec{V} \cdot \nabla_p)\vec{V}_g + w\frac{\partial \vec{V}_g}{\partial z} \right), \tag{2.15}$$

where the convergence term is defined as $\nabla_p = \left(\frac{\partial}{\partial x}, \frac{\partial}{\partial y}\right)_p$ on levels of equal pressure. The first term between the brackets represents the isallobaric wind, the second term refers to the advection of the real wind by the geostrophic wind and the third term represents the inertial convective component. The first term of this equation can be expanded with the definition of the geostrophic wind, which is given by equation 2.9, so that this term becomes,

$$\vec{V}_{isa} = \frac{\hat{k}}{f} \times \frac{\partial \vec{V}_g}{\partial t} = \frac{\hat{k}}{f} \times \frac{\partial}{\partial t}\left(\frac{g\hat{k}}{f} \times \nabla_p z \right). \tag{2.16}$$

The gravitational acceleration and Coriolis parameter can be assumed to be constant in time and therefore could be placed out of the time derivative in this equation. The vertical unit vector is also constant in time, with therefore can be placed into the time derivative, so the equation becomes,

$$\vec{V}_{isa} = \frac{g}{f^2}\frac{\partial}{\partial t}\left(\hat{k} \times (\hat{k} \times \nabla_p z) \right). \tag{2.17}$$

With the rule that $\hat{k} \times (\hat{k} \times \nabla_p z) = -\nabla_p z$, the equation becomes,

$$\vec{V}_{isa} = \frac{g}{f^2}\frac{\partial}{\partial t}(-\nabla_p z). \tag{2.18}$$

By reversing the tendency and the convergence, the ageostrophic wind can be written as,

$$\vec{V}_{isa} = -\frac{g}{f^2}\nabla_p \left(\frac{\partial z}{\partial t} \right). \tag{2.19}$$

This component of the ageostrophic wind is called the isallobaric wind, which is caused by the gradient of pressure tendency. The isallobaric wind is directed down the gradient of pressure tendencies, as is illustrated in figure 2.3.

In areas of fast deepening or fast moving cyclones, rapidly building or fast moving anti-cyclones the isallobaric wind can be large. The geostrophic and isallobaric wind re-enforce

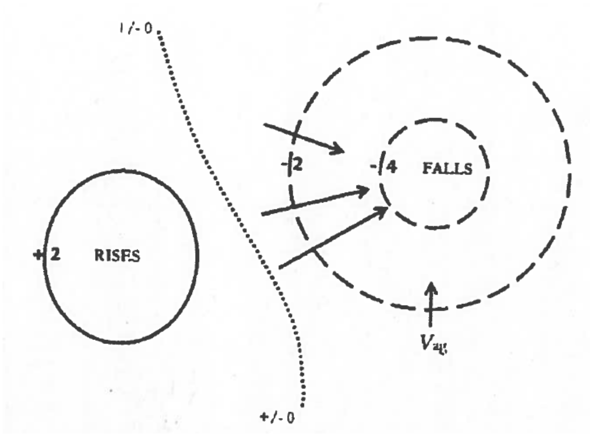

Figure 2.3: The illustration of the direction of the ageostrophic wind, which is pointed from pressure rises to pressure falls [6].

each-other in the southern area of a cyclone and counteract each other in the northern area of a cyclone it the cyclone moves eastward [9, 170-173], [6].

The second term of equation 2.15 gives the inertial-advective component of the ageostrophic wind, which is the horizontal advection of the geostrophic wind by the real wind. This term can be expanded into Cartesian coordinates, resulting in,

$$\frac{\hat{k}}{f} \times \left[\left(u\frac{\partial u_g}{\partial x} + v\frac{\partial v_g}{\partial y} \right) \hat{\imath} + \left(u\frac{\partial v_g}{\partial x} + v\frac{\partial v_g}{\partial y} \right) \hat{\jmath} \right], \tag{2.20}$$

where $\hat{\imath}$ and $\hat{\jmath}$ are the unit vectors in the x- and y-direction. The vector notation can be written out as,

$$u_{iner} = \frac{1}{f} \left(u\frac{\partial v_g}{\partial x} + v\frac{\partial v_g}{\partial y} \right) \tag{2.21}$$

$$v_{iner} = \frac{1}{f} \left(u\frac{\partial u_g}{\partial x} + v\frac{\partial u_g}{\partial y} \right), \tag{2.22}$$

where the gradient in the geostrophic wind determines the inertial advective component of the ageostrophic wind. In the situation of a trough the geostrophic wind is pointing from west to east, this is illustrated in figure 2.4. The inertial advective component of the ageostrophic wind is in this case directed in the opposite direction to the geostrophic wind. This wind will be strong in regions of diffluent or confluent flow, curved flow (ridges and troughs) or in the entrance/exit region of the jet stream [4] [9, page 170-173] [6].

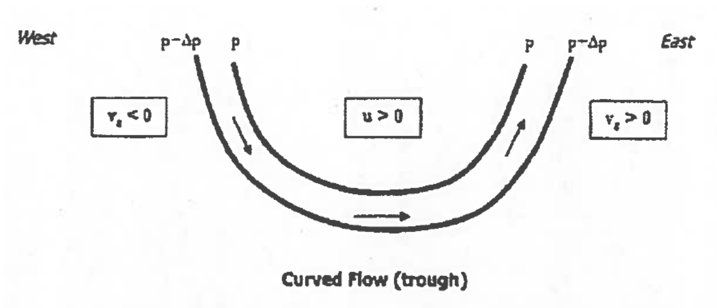

Figure 2.4: The curved flow in a through, where the inertial advective wind is directed in opposite direction of the geostrophic wind following the arrows [6].

2.3 Wind profiler

The wind profiler makes use of the RADAR (RAdio Detecting And Ranging) technology, which transmits a pulse of energy in a selected direction and then detects the return of the signal. The time delay between transmission and reception of the signal determines the distance to the target. The wind profiler is shown in figure 2.5, which also illustrates the direction of the pulses.

The wind profiler depends on the scattering of the transmitted electromagnetic energy by irregularities in the refractive index of the air. These irregularities in the refractive index are induced by small variations in the wind, which produce eddies. The refractive index in the lower atmosphere depends on the temperature, pressure and humidity. Eddies are small, whirling currents of air and are created over a wide range of sizes, from centimeters to tens of meters. Eddies tend to break up into smaller eddies. At the smallest size of the eddies, the break up is replaced by dissipation of energy by viscous heating. These small eddies produce the small variations in the refractive index of the air, which initiate scattering. Backscattering of the signal occurs from irregularities of a size of one-half the wavelength of the radio wave (Bragg scattering). The small eddies are carried by the wind, from which the wind speed can be determined.

The wind profiler transmits short pulses of radio energy in a selected direction and with a selected wavelength. To detect scattering at the receiver, the wavelength of the pulse must also be in the cm to m range. The return signal is received from all heights within the range of the wind profiler, which is from 137 m up to 7 km. Return signals from equally spaced heights are obtained by sampling the return signal at equal spaced times.

The transmitted pulse has a finite length, so the received signal is coming from a volume of the atmosphere. In low (high) mode the wind profiler measures every 60 m (200 m) in a height range of 100 m (400 m).

The transmitted pulse with a frequency of 1290 MHz is sent in a beam in a specific direction. If a volume of air has a motion towards or away from the radar, the returned signal is shifted in frequency. From the Doppler effect it is known that the shift in the frequency is proportional to the speed of the air.

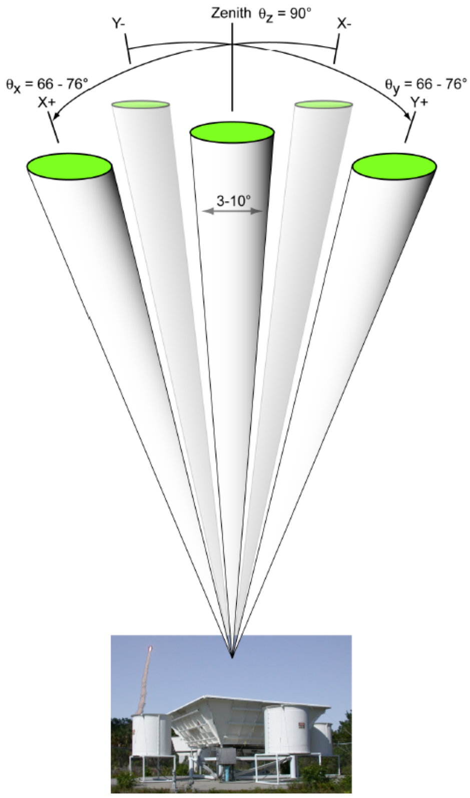

Figure 2.5: The wind profiler with the five directions of the beam [10].

By measuring the frequency shift, the radial velocity can be determined. At least three directions are needed to calculate the wind, but five directions are used by the wind profiler to provide a better quality of the data. The wind profiler uses four orthogonal off-zenith beams, and one beam in the vertical direction. The beam is pointed in high elevation angles to represent the same flow regime [10].

Chapter 3

Quality Mode-S EHS data

The Mode-S EHS data is used to derive the wind speed and wind direction, but in order to use this data, the quality of the data must be known. This chapter is divided into three parts and describes the validation of the quality of the Mode-S EHS data. The first section focusses on the Mode-S EHS data and how this data is processed to investigate the quality of the Mode-S EHS data. The second section, which is focused on the comparisons set-up, explains how the Mode-S EHS data is compared with the KNMI Cabauw tower and the wind profiler situated at Cabauw. The third section reveals the results of the comparisons and the conclusion if the Mode-S EHS data is valuable to use for further research.

3.1 The Mode-S EHS data

Every four seconds the Mode-S EHS radar requests information from all the aircrafts in its range. In areas where radars overlap each other, the aircraft data is requested with a higher frequency. Figure 3.1a shows all the aircraft tracks of the Mode-S EHS equipped radars on the 28 of October 2013. It can be seen that the airspace contains a couple of highways, with a lot of aircrafts flying in these regions. This means that the airspace above the Netherlands is busy and nearly covers the whole country.

The area around Amsterdam Schiphol airport is a representative location to investigate the storm of the 28 of October 2013, because of the wide range of flight levels. The location of Schiphol is at longitude $\lambda = 4.77°$ and latitude $\phi = 52.31°$, but to contain enough aircraft measurements for the comparisons, a box is drawn around Schiphol. The area around Schiphol lies between longitude 4.5° E and 5.0° E and between latitude 52.0° N and 52.5° N. Figure 3.1b shows all the aircrafts which cross the area around Schiphol or did take off from- or did land at Schiphol airport during the storm of the 28 of October 2013. During this day, the aircrafts mostly landed from northern and eastern direction, while they took-off in the southern direction. The blue lines in figure 3.1b indicate the aircrafts which are landing or taking off from the airport, the red dots instead, show the aircrafts which are flying at high altitudes over this region. The thick blue lines indicate the most common routes on this day.

The Mode-S EHS data from the aircrafts contains information of flight level (F), Mach number (M), roll, true airspeed (V_t), heading (α_t), ground speed (V_{gr}) and ground track angle (α_{gr}). With this information, the wind speed can be determined with the use of equation 2.2. Aircraft which are turning are filtered out of the data, because the uncertainty in the calculation of the wind speed is larger when the aircraft has a roll. The reprocessed data

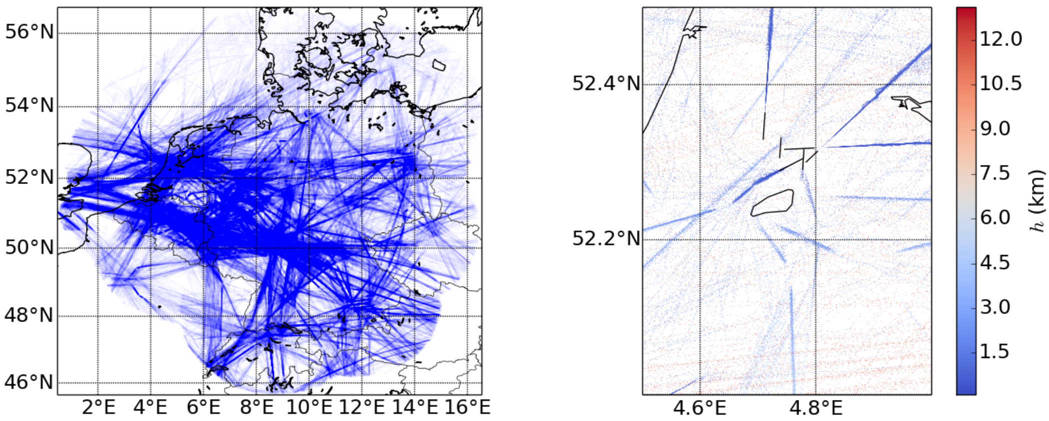

(a) (b)

Figure 3.1: All aircraft tracks on 28 October 2013 within the Mode-S EHS data, with for (a) the total area and for (b) only the box around Schiphol.

contains information about the date, time in UTC, aircraft-code, latitude, longitude, flight level in feet, wind speed in knots, wind direction in degrees, temperature in Kelvin and information whether the aircraft is rising, descending, or flying at constant flight-level.

The flight level of the aircrafts is calculated from the pressure-level measured by the aircrafts. A standard atmosphere as defined by the ICAO (International Civil Aviation Organization) is assumed to determine the flight level, which defines how the pressure, temperature and density of the atmosphere change as function of the altitude. In this standard atmosphere a surface pressure of 1013.25 hPa is assumed for the calculation of the flight level of the aircraft. With a surface pressure which is not constant over time, the flight level does not match with the real height of the aircraft. To determine the real height of the aircraft, a conversion is made to determine the true height of the aircraft. The pressure-altitude of the aircraft determined from the flight level can be written as,

$$p(F) = p_0 \left(\frac{T_0 - \Gamma F}{T_0} \right)^{g/\Gamma R_d}, \tag{3.1}$$

where p_0 is the pressure at sea level ($p_0 = 1013.25\,\mathrm{hPa}$), T_0 is the standard temperature at sea level ($T_0 = 288.15\,\mathrm{K}$), F is the flight level of the aircraft in m and Γ is the atmospheric lapse rate ($\Gamma = 0.0065\,\mathrm{Km}^{-1}$). The derivation of this equation is explained in Appendix D. The flight level can also be corrected for the pressure at sea level, for example for the area around Schiphol. The correction height is defined as,

$$h_{corr} = -\frac{T_0}{\Gamma} \left(\left(\frac{p_1}{p_0} \right)^{\left(\frac{\Gamma R_d}{g} \right)} - 1 \right), \tag{3.2}$$

where p_1 is the pressure-altitude of the aircraft and p_0 is the measured surface pressure. So the 'real' height of the aircraft is defined as the flight level minus the correction height.

3.2 Comparisons set-up

The quality of the Mode-S EHS data is validated for further research. The Mode-S EHS data is compared with a wind profiler situated at Cabauw, the KNMI (Royal Dutch meteorological Institute) Cabauw tower and the Harmonie version 36 weather model of the KNMI. Cabauw is situated in the Green heart, which is a representative area for the Netherlands with agriculture and open terrain around the tower, surrounded by urban areas of the neighborhood. The KNMI Cabauw tower is a measurement facility for research to the atmospheric boundary layer. The exact location of the Cabauw tower is at longitude $\lambda = 4.93°$ and at latitude $\phi = 51.97°$ and is situated at a distance of 39 km from Amsterdam Schiphol airport. The wind profiler is located at a distance of 200 m from the Cabauw tower. The Mode-S EHS data is compared with the Cabauw tower and the wind profiler for the month October 2013 and thus contains the storm of the 28 of October 2013.

3.2.1 Configuration of the data

The three observing systems are configured differently, which also requires some processing of the data before they can be compared with each other. Table 3.1 shows the configuration of the data from the three measurement devices, which shows the format of the time, position, height, wind speed and wind direction.

Table 3.1: The configurations of the Mode-S EHS data, the wind profiler and the Cabauw tower

	Mode-S EHS	Wind profiler	Cabauw tower
Time	point measurement	30 minute average	10 minute average
Position	λ (°), ϕ (°)	-	-
Height	F (feet)	h (m)	h (m)
Wind speed	V (knots)	u, v, V (ms^{-1})	V (ms^{-1})
Wind direction	d (°)	d (°)	d (°)

The measurement height of the aircrafts is determined from the pressure of the atmosphere and the assumption of a standard atmosphere of the ICAO with a surface pressure of 1013.25 hPa. The Mode-S height is converted to pressure levels with the use of equation 3.1 which corrects for the surface pressure. With the help of equation 3.2 and the surface pressure measured at Schiphol airport, which is setup as 10 minute average data, the height of the aircrafts can also be determined in meters. The Mode-S EHS data is compared with the other devices in pressure altitude. The pressure surface of the measurement levels of the Cabauw tower and the wind profiler can be determined with the use of equation 3.1 and the measured surface pressure at Cabauw (p_0). The pressure at Cabauw is given as 10 minute average data.

To determine the mean wind direction of several measurements, this should be done by first taking the mean of the u- and v-component of the wind, and then determine the wind direction from the wind components. The data of the Mode-S EHS and the Cabauw tower only give the total wind vector and the wind direction. The u- and v-components of the wind can be determined by,

$$u = -V \cdot \sin\left(d\frac{\pi}{180}\right) \tag{3.3}$$

$$v = -V \cdot \cos\left(d\frac{\pi}{180}\right), \tag{3.4}$$

where the minus term is added to convert for the definition of the wind direction which is defined as the direction where the wind blows from. To determine the total wind speed from the u- and v-component of the wind, the sum of the vector length determines the total wind speed, written as,

$$V = \sqrt{u^2 + v^2}. \tag{3.5}$$

The mean wind direction of the Mode-S EHS measurements is determined from the mean u and v component of the wind written as,

$$d = \tan^{-1}\left(\frac{u}{v}\right) \cdot \frac{180}{\pi}. \tag{3.6}$$

3.2.2 Mode-S EHS vs. wind profiler

The wind profiler measures in a wide range of heights up to 7 km height and has two measurement configurations. In the low mode, the wind profiler measures in the lower 1500 m of the atmosphere. In high mode, the wind profiler measures at higher altitudes. The wind profiler measures the wind speed and wind direction as a function of height in a time interval of 30 minutes.

The altitude of the airplanes is determined in pressure levels and the measurement levels of the wind profiler are given in geometric levels. To compare these two measuring devices, the wind profiler height should be converted to pressure levels. The surface pressure is measured at the Cabauw tower as ten minute average data, which can be converted to half hour average data. With the pressure at the surface, the pressure can be calculated for different measurement altitudes of the wind profiler. With the assumption of a standard atmosphere and the use of equation 3.1, the pressure level of the wind profiler heights can be calculated, where F is the measurement height and p_0 is the measured surface pressure.

The wind profiler measures the wind speed in a height range, instead of one single point. In low mode the wind profiler measures in steps of 60 m with a height range of $\Delta h = \pm 50$ m. In high mode the wind profiler measures in steps of 200 m with a height range of $\Delta h = \pm 200$ m, so the different measurement levels overlap each other. The quality of the wind profile data is checked by the software and by an expert, they flag the data when it is invalid.

The Mode-S EHS data is categorized in the same format as the wind profile data, so per height and time range. All the measurements of the aircrafts in this range are averaged to compare the Mode-S EHS data with the wind profile data. The minimum number of measurements is set to 10 to get a mean value of the Mode-S EHS data, instead of one measurement. Wind speeds lower then 4 ms^{-1} are not taken into account in the comparison of the wind direction, because the determination of the wind direction becomes uncertain at lower wind speeds.

3.2.3 Mode-S EHS vs. Cabauw tower

The Cabauw tower is a 200 m high meteorological measurement mast, with on several levels instruments which measure the wind speed. The mast is build up with 6 measurement levels with on every level 3 measuring arms. Each arm has measurement devices which measure amongst other the wind speed, wind direction and temperature. Figure 3.2 shows the KNMI Cabauw tower and illustrates the three arms and the different measuring levels. The wind speed and wind direction are chosen from the arm which is in the direction where the wind is least affected by the flow around the tower.

Figure 3.2: The KNMI Cabauw tower.

The 3 highest levels of the Cabauw tower are used to compare with the Mode-S EHS data, which are at 80, 140 and 200 m. To compare the Cabauw tower data with the Mode-S EHS data, a height range around the tower level are taken into account to get some aircraft data. It is chosen to set the range to $\pm$ 20 m around the measurement levels of the tower. The tower levels and ranges are converted to pressure altitude with the use of equation 3.1. All the aircrafts in the height and time range are averaged, with a minimum of 5 measurements to compare to average measurements of the wind speed and wind direction.

3.2.4 Wind profiler vs. Cabauw tower

The Cabauw tower and the wind profiler are also compared with each other, to determine the difference between the two measurement facilities. The Cabauw tower level at 140 m is linked with the mean measurement height of 137 m of the wind profiler to compare both facilities. The Cabauw tower level of 200 m is linked with the wind profiler height of 195 m. To compare these measurement devices, the three 10 minute average measurements are averaged to get the same half hour mean as the wind profiler.

3.2.5 Mode-S EHS vs. Harmonie 36

The Mode-S EHS data is also compared with the output of the Harmonie 36 model of the KNMI for the 28 of October 2013. Harmonie is solved in gridpoints and each grid box has a spatial size of 2.5 by 2.5 kilometers. The model predicts the weather for the Netherlands from longitude 0° E to 11° E and for latitude 49° N to 56° N, which contains 300 by 300 gridpoints. Harmonie 36 solves the meteorological parameters at 60 levels of the atmosphere, where the pressure level at 800 hPa is used for the comparison. The output from the model which is used are the u and v components of the wind. The model is not initiated with the Mode-S EHS measurements, to show a real comparison between Harmonie 36 and Mode-S EHS.

The Mode-S EHS data is not only compared for the area around Schiphol, but for the whole Netherlands. The model output is given for every hour, which gives the instant value of the wind components. Every grid box of the Harmonie 36 model in the Netherlands is used in the comparison. Aircrafts flying in a time range of $\mathrm{d}t = \pm 10$ minutes around the Harmonie 36 time and a pressure range of $\mathrm{d}p = \pm 20$ hPa around a pressure level of 800 hPa in one of the grid boxes of the model, are included in the comparison with the Harmonie 36 model. Minimal 5 aircraft measurements are needed per Harmonie grid box for the comparison.

3.3 Results

This section discusses the results of the evaluation of the Mode-S EHS data, by discussing the results of the comparison of the Mode-S EHS data with the wind profiler and the Cabauw tower. To check the similarity between the Cabauw tower and the wind profiler, these two data sets are also compared with each other.

3.3.1 Comparison between Mode-S EHS and wind profiler

The Mode-S EHS data is compared with the wind profiler to investigate the quality of the Mode-S EHS data in a wide range of heights in the atmosphere. The wind profiler can measure the wind until a height of 7 km, which gives the opportunity to validate the Mode-S EHS data over a wide range of heights. Figure 3.3 shows the scatter plot of the Mode-S EHS data as function of the wind profile data, with for (a) the wind speed and for (b) the wind direction. The number of measurements used for the comparison between the two measurement techniques is 25899 for the wind speed and 23810 for the wind speed direction.

The scatter plot of the wind speed is given in figure 3.3a, which gives in the upper left corner of the figure the quality of the comparison between the two measuring techniques. The slope of the scatter plot is $s = 1.04$ with a correlation coefficient of $R^2 = 0.884$. The symbol Δ gives the mean difference between the two measurement techniques with the y-axis minus the x-axis, symbol σ gives the standard deviation in the difference between the two measurement techniques, and n gives the number of measurements which are used in the comparison.

The mean bias between the two measuring techniques is $\Delta = 0.764$ ms^{-1}, which means that as a whole the Mode-S EHS measures 0.764 ms^{-1} higher wind speeds then the wind profiler. The standard deviation in the bias is $\sigma = 2.27$ ms^{-1}, this means that the spread in the data is quite small in the wide range of measured wind speeds.

Figure 3.3b shows the scatter plot of the wind direction for the Mode-S EHS as function of the wind profiler. It shows that the slope of the scatter plot is $s = 0.998$ with a correlation

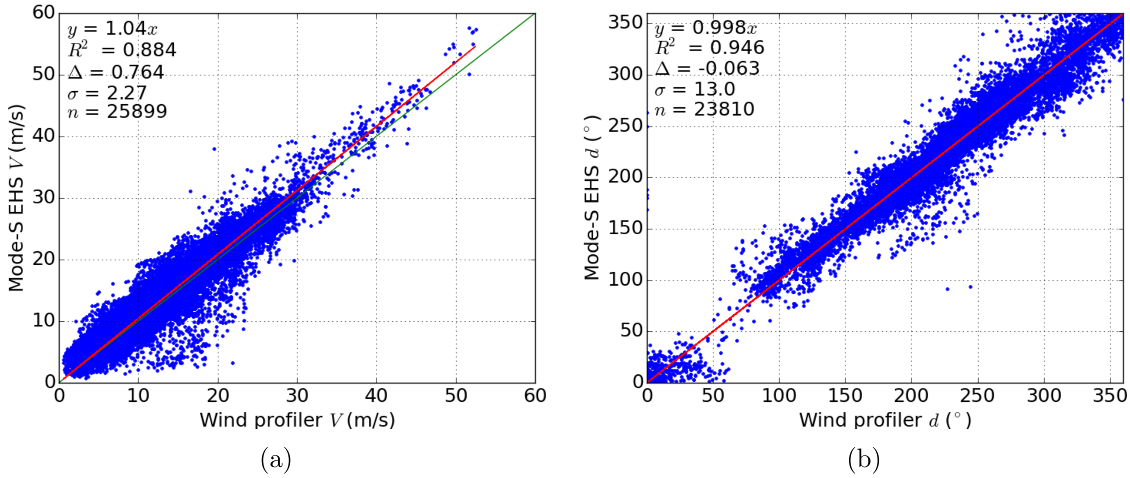

Figure 3.3: The scatter plot for the month October 2013 for the Mode-S as function of the wind profiler for (a) the wind speed and (b) the wind direction.

coefficient of $R^2 = 0.946$. The bias in the wind direction is $\Delta = -0.063°$ with a standard deviation of $\sigma = 13.0°$.

As was mentioned in the introduction to section 3.2, the distance between Cabauw and Schiphol is 39 km. So with the correlation coefficient around 0.9, the small bias between the two devices and the small spread in the comparison between the two, it can be concluded that the Mode-S EHS and the wind profiler compare good with each other. Therefor, the correspondence is surprisingly good.

3.3.2 Comparison between Mode-S EHS and Cabauw tower

This subsection presents the results from the comparison between the Mode-S EHS and the Cabauw Tower. Due to the height of this tower, it is possible to compare the Mode-S EHS data in the area around Schiphol with the Cabauw tower data. The comparison between the two instruments takes place over the month October 2013.

Figure 3.4 shows the comparison for the Mode-S EHS as function of the Cabauw tower with for (a) the wind speed and for (b) the wind direction. The number of measurements used in the comparison is 1248 for the wind direction, and 1303 for the wind speed. This comparison contains less data then the comparison with the wind profiler, because in the comparison with the Cabauw tower, only measurement level at 80, 140 and 200 m are used.

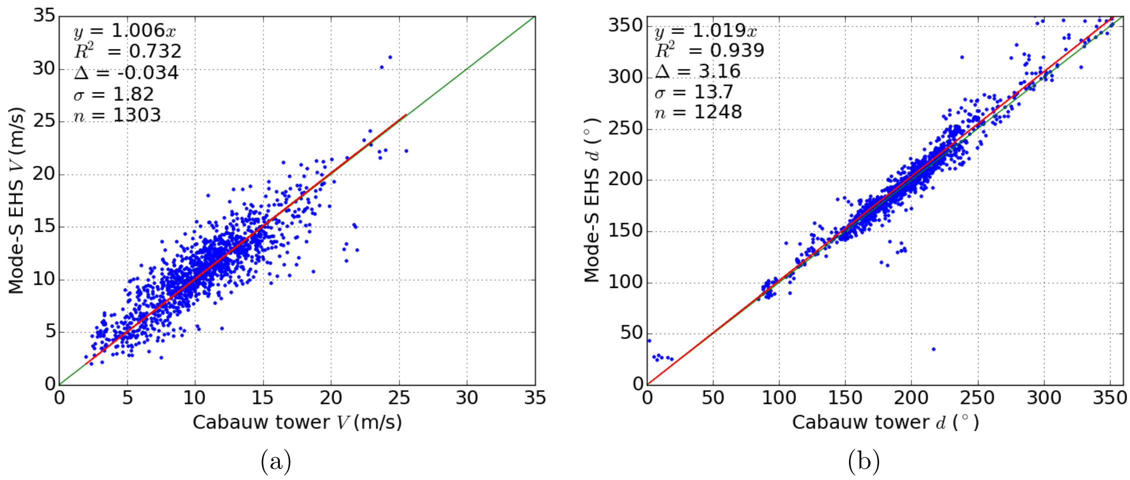

Figure 3.4: The scatter plot for the month October 2013 for the Mode-S as function of the Cabauw tower with for (a) the wind speed and (b) the wind direction

Figure 3.4a shows the scatter plot of the wind speed for the Mode-S EHS as function of the Cabauw tower. It shows that the slope of the scatter plot is $s = 1.006$ with a correlation coefficient of $R^2 = 0.732$. The bias in the Mode-S EHS data in comparison with the Cabauw tower is $\Delta = -0.034$ ms^{-1} with a standard deviation of $\sigma = 1.82$ ms^{-1}. So the wind speed measured by the Mode-S data is in the same order as the Cabauw tower with a range of 2 ms^{-1}. The correlation coefficient is found to be lower than in the comparison with the wind profiler, this can be explained by the smaller range of wind speeds in the comparison with the Cabauw tower, which results in a relative larger spread of the scatter plot.

Figure 3.4b shows the scatter plot of the wind direction for the comparison of the Mode-S EHS data as function of the Cabauw tower. The slope of the scatter plot is $s = 1.019$ with a correlation coefficient of $R^2 = 0.939$. The bias in the wind direction of the Mode-S EHS in comparison with the Cabauw tower is $\Delta = 3.16°$ with a standard deviation of $\sigma = 13.7°$. So the Mode-S EHS measures a 3° wider range of directions then the Cabauw tower in a range of 14°. Cabauw is situated more inland than Schiphol, which induces more friction and could explain the differences in the observing systems.

3.3.3 Comparison between Cabauw tower and wind profiler

The Wind profiler and the Cabauw tower are also compared with each other to validate the quality of the two measurement devices. Figure 3.5 shows the scatter plot of the wind profiler as function of the Cabauw tower with for (a) the wind speed and for (b) the wind direction. The Cabauw tower measurement is set on the horizontal axis, because this measurement facility is seen as the reference meteorological location of the Netherlands. The comparison contains 2655 data points for the wind speed and 2370 data points for the wind direction.

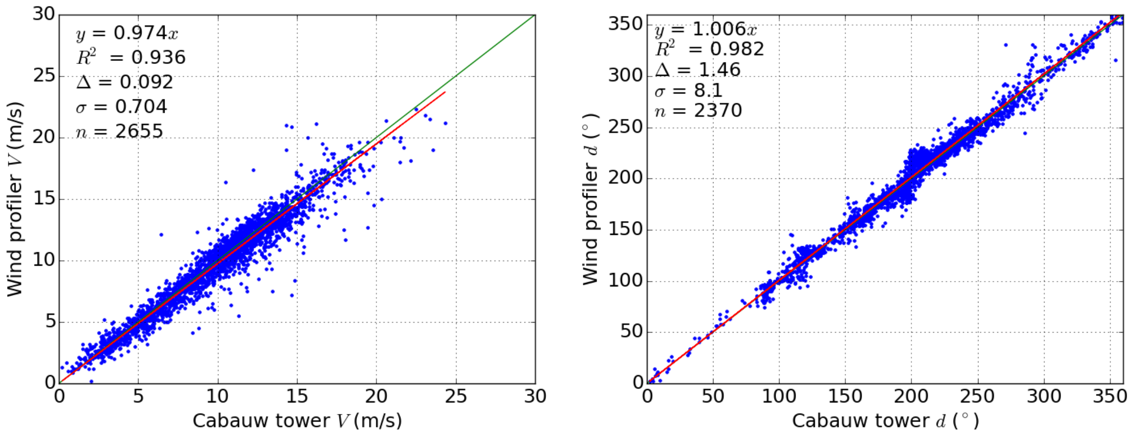

(a) (b)

Figure 3.5: The scatter plot for the month October 2013 for the wind profiler as function of the Cabauw tower with for (a) the wind speed and (b) the wind direction.

Figure 3.5a shows the scatter plot of the wind speed with the wind profiler as function of the Cabauw tower. The slope of the scatter plot is $s = 0.974$ with a correlation coefficient of $R^2 = 0.936$. The bias of the wind profiler in comparison with the Cabauw tower is $\Delta = 0.092$ with a standard deviation of $\sigma = 0.704$.

Figure 3.5b shows the scatter plot of the wind direction with the wind profiler as function of the Cabauw tower. The slope in the plot is $s = 1.006$ with a correlation coefficient of $R^2 = 0.982$. The bias in the wind direction is $\Delta = 1.46°$ with a standard deviation of $\sigma = 8.1°$. The wind profiler measures a wider range of wind directions of 1° with a range of 8°.

The differences between the wind profiler and the Cabauw tower can be explained by the different measurement techniques. The wind profiler measures the wind a couple of times in 30 minutes and then determines an average wind speed of these measurements. The wind instruments at the Cabauw tower measure the wind speed continuously and averages over the whole 10 minute range. The measurement levels used for this comparison are 140 m and 200 m for the Cabauw tower and 137 m and 195 m for the wind profiler. The wind profiler measures the wind speed as a range of 60 m around the measurement level, where the Cabauw tower measures the wind at the specific level.

3.3.4 Comparison between Mode-S EHS and Harmonie 36

The Mode-S EHS data is compared with the Harmonie 36 weather model of the KNMI to determine if the model predicts the same wind as the measured wind. Due to the large data output files of the Harmonie model, the wind is only compared for 28 of October 2013. Figure 3.6 shows the scatter plot of Mode-S EHS as function of Harmonie 36 for (a) the wind speed and for (b) the wind direction. The comparison contains 652 data points, for both the wind speed and wind direction.

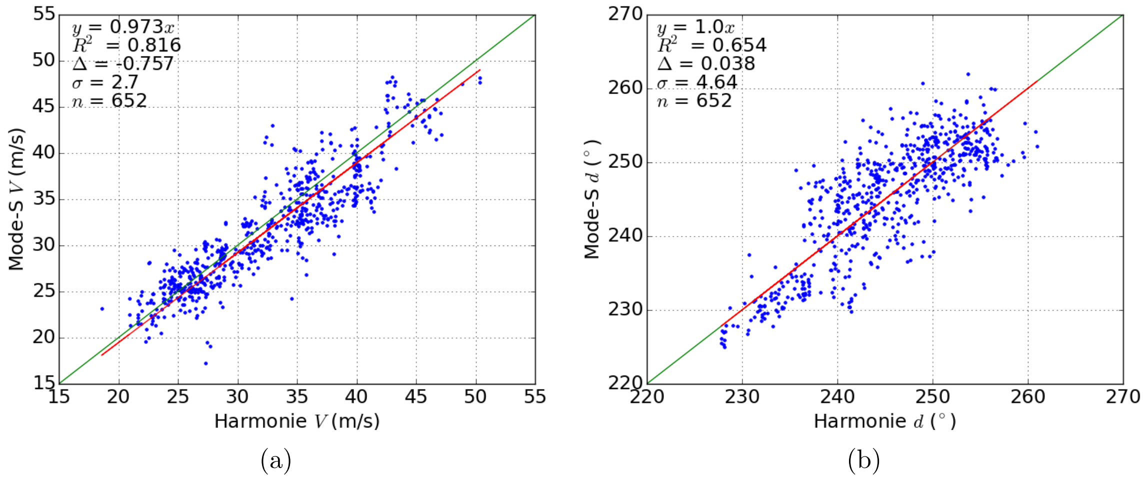

Figure 3.6: The scatter plot at 25-30 October 2013 for the wind profiler as function of the Cabauw tower with for (a) the wind speed and (b) the wind direction.

Figure 3.6a shows the scatter plot of the wind speed with the Mode-S EHS as function of the Harmonie 36. It shows that the slope of the scatter plot is $s = 0.973$ with a correlation coefficient $R^2 = 0.816$. The Mode-S EHS data measures overall $\Delta = 0.757$ lower then Harmonie 36 with a standard deviation of $\sigma = 2.7$ ms^{-1}. The wind direction, shown in figure 3.6b, shows a slope of 1.0 with a correlation coefficient of $R^2 = 0.654$. The bias between the two is also small with a $\Delta = 0.038$ and a standard deviation of $\sigma = 4.64°$.

The wind speed and the wind direction measured by Mode-S EHS and Harmonie 36 shows a good correlation. The difference in the wind speed between the Mode-S EHS and Harmonie 36 can be explained by the fact that the Harmonie 36 is just an instant value, and the Mode-EHS is an average of minimal 5 wind measurements. So this influences the comparison between the Mode-S EHS and Harmonie 36.

The comparison of the Mode-S EHS with the other measurement techniques shows a good correlation. Also with the knowledge of the large distance of 39 km between Schiphol and Cabauw, it can be concluded that the Mode-S EHS data can be used for further research.

Chapter 4

Storm of the 28 of October 2013

The storm of the 28 October 2013 is of interest due to the large wind gusts measured over the Netherlands, in particular in the northern parts of the country. This chapter is devided into six paragraphs with a case study of the storm. The first section describes the storm of the 28 of October 2013. The second section discusses the wind during the storm, according to the Mode-S EHS data. The third section explains the first method in determining the theoretical wind, which also contains the two methods used to determine the theoretical wind, namely the piecewise linear interpolation method and the finite difference method. The fourth section describes the first results in the calculation of the wind speed and shows that the method should be optimized. The fifth section describes the new methods to determine the theoretical wind, where the results of theoretical wind are discussed in the sixth part.

4.1 Case description, the 28 of October 2013

The storm of the 28 of October 2013 broke the Dutch record for the highest wind gust for the month of October at three locations. A wind gust of 148.2kmh^{-1} was measured on Texel, 151kmh^{-1} was measured on Vlieland and the strongest wind gust of 152kmh^{-1} was measured at Lauwersoog. Such large wind gusts have a repetition time of 30 years. The storm was formed in the Western Atlantic as a secondary low south of a large low pressure area located south east of Greenland. The combination of a strong jet stream, the remnants of an ex-tropical cyclone and a small perturbation in the isobars caused a strong cyclone [11].

Figure 4.1 shows the airmass RGB of a satellite product which shows the airmass of a volume of air for 27 October 2013 at 12:00 UTC. The dark blue color indicates cold air masses, the blue-green color indicates warm air masses and the red color indicates areas of dry descending stratospheric air into the troposphere. Two model levels are plotted over the airmass RGB, where the green lines show the geopotential height of the 500 hPa pressure level, and where the yellow lines show the cyclonic vorticity advection, which is the result of more cyclonic values of vorticity advecting into lower values of vorticity. The airmass RGB shows a small trough on the left side of the figure west of the United Kingdom seen by the curvature in the lines of equal geopotential height at 500 hPa. This trough introduces positive vorticity advection due to cyclonic curvature in the lines of equal geopotential height. Just west of the curvature in the lines of equal geopotential height, an area of high positive vorticity advection is illustrated by the yellow lines. Stream upwards of the trough the cold air is well visible, as well as the red colors indicating dry descending stratospheric air into the troposphere.

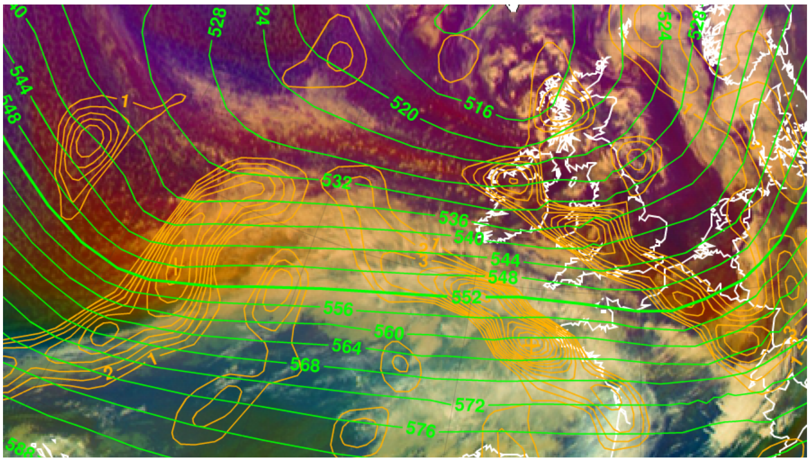

Figure 4.1: The airmass RGB of 27 October 2013 for 12:00 UTC [15]. The dark blue colors indicate cold air masses, the blue/green colors indicate warm air and the red color indicate dry descending stratospheric air. The green lines show the geopotential height of the 500 hPa pressure level and the yellow lines show the cyclonic vorticity advection.

The secondary low at the surface on 27 October 2013 at 12:00 UTC was located east of the large area with vorticity advection and west of number 556 in figure 4.1. 12 hours later the secondary low at the surface did move in the western direction situated between Wales and Ireland. Figure 4.2 shows the airmass RGB for 28 October 2013 at 00:00 UTC, where the secondary low at the surface did move with a velocity of 80 km/h from the Atlantic in the direction of the United Kingdom. The trough did build up in 12 hours and a small ridge is visible between France and the United Kingdom. Between the trough and the ridge the air parcels accelerate under influence of the large temperature gradient from north-west to south-east, indicated as the position of the jet streak. The trough induces positive vorticity advection located west of the trough, also illustrated by the yellow lines south of Ireland. An large area of dry descending stratospheric air is visible from the left-down corner of the figure descending into the air just south of Ireland. This physical processes did result in a fast moving and fast deepening of the cyclone.

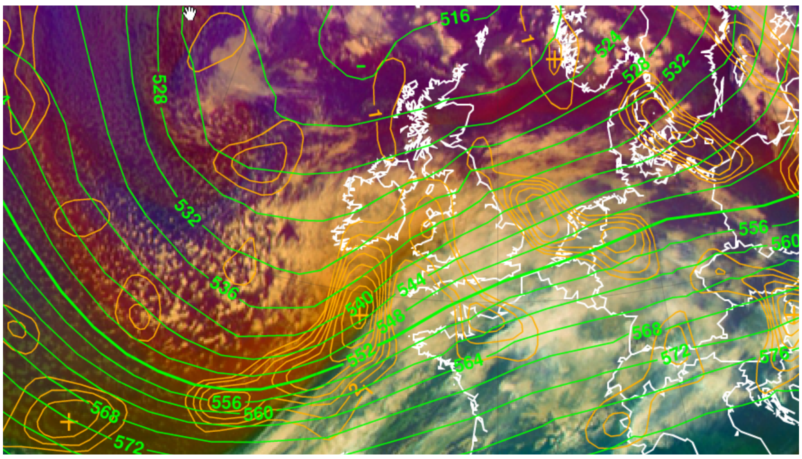

Figure 4.2: The airmass RGB of 28 October 2013 for 00:00 UTC [15].

Figure 4.3 shows the satellite image of the water vapor channel with wavelength 6.2 μm for 28 October 2013 at 06:00 UTC. In this satellite channel the black color indicates dry air, the gray color indicates humid air and the white color shows high clouds and cirrus clouds. The satellite image shows a dry intrusion of air from the stratosphere into the troposphere just west of the Netherlands. A thick layer of clouds is situated above the Netherlands and the North Sea at this time. The jet streak is situated in the transition between bright and dark colors, situated just west of France.

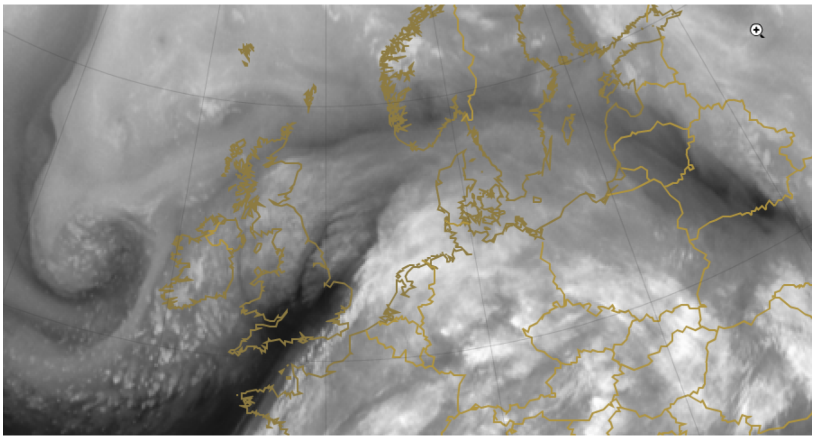

Figure 4.3: The satellite image of the water vapor channel 6.2 μm of 28 October 2013 for 06:00 UTC [15].

Figure 4.4 shows the satellite image of the water vapor channel with wavelength 6.2 μm for 28 October 2013 at 12:00 UTC. At this time the center of the cyclone is situated just North East of the Netherlands. A line of high clouds is situated over Western Europe extending from the East of the Netherlands to the South of France. The occlusion band is situated west around the dark area in the image. The position of the jet stream can also be seen from the satellite image which is situated in the dark gray area between West European mainland and the United Kingdom. The dry intrusion of the stratospheric air is situated above Denmark.

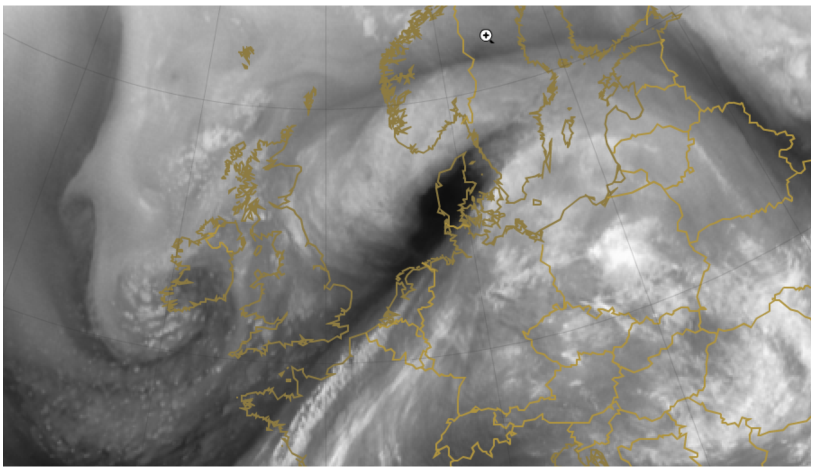

Figure 4.4: The satellite image of the water vapor channel 6.2 μm of 28 October 2013 for 12:00 UTC [15].

Figure 4.5 shows the weather maps of Europe on 28 October 2013, with for sub figure 4.5a at 06:00 UTC and 4.5b at 12:00 UTC. At 06:00 UTC the disturbance in the isobars formed a low pressure core, which deepened at 12:00 UTC. North-east of the center of the storm a warm front was passing the Netherlands with a large rain area. Figure 4.6 shows the rain radar of the Netherlands for 28 October 2013 for different times of the day. At 06:00 UTC the warm front is situated in Northern part of the Netherlands bringing a large area with precipitation illustrated in sub figure 4.6a. The rain radar also shows some showers in the South East part of the country.

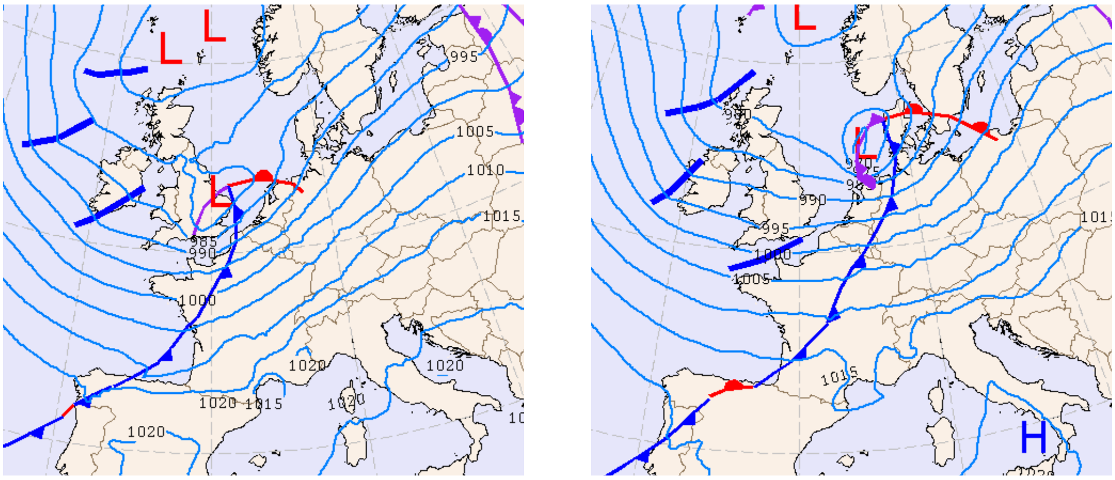

(a) (b)

Figure 4.5: The weather maps of 28 October 2013 with analyses from the KNMI, with for (a) 06:00 UTC and (b) 12:00 UTC.

The weather maps show a cold front extending from the North Sea to the south of France. This cold front makes the atmosphere potential unstable and when the cold front passed the east of the Netherlands it produces a line of showers. Sub figure 4.6b illustrates the rain showers at 10:00 UTC above the Netherlands where on the cold front a line of showers were produced. The occlusion moved just west of the center of the low pressure area as seen in figure 4.5. The curved occlusion was also accompanied with a rain area, which is good visible in the rain radar of 10:00 UTC shown in sub figure 4.6b.

At 12:00 UTC the isobars in the Northern part of the Netherlands are close to each other, which causes strong geostrophic winds in this area. The rain at 12:00 UTC in sub figure 4.6c shows that the air after the cold front is potential unstable and some showers are produced which follow the lines of curvature of the isobars. The occlusion is visible north west of the Netherlands on the North Sea [13], [14].

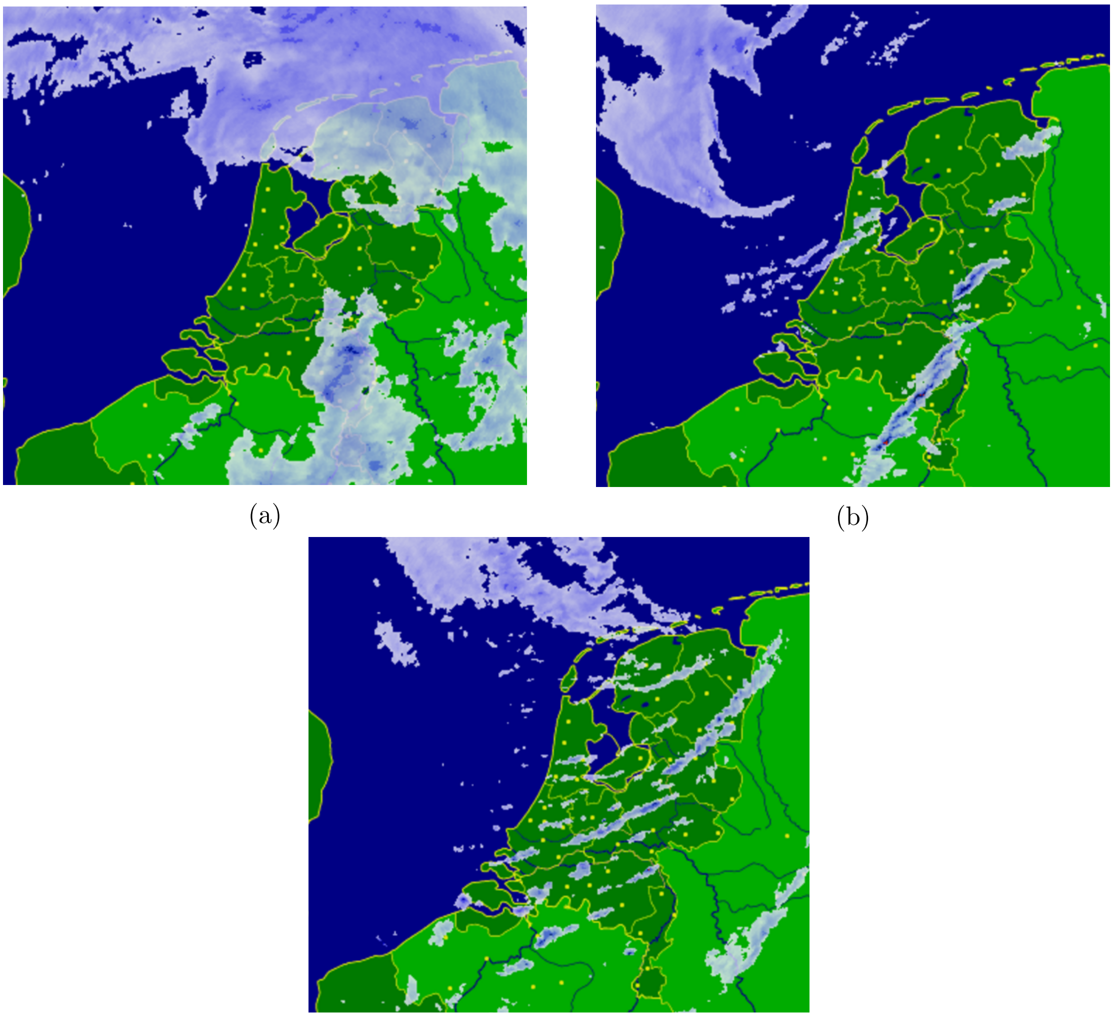

(a) (b) (c)

Figure 4.6: The rain radar of 28 October 2013 with for (a) 06:00 UTC, (b) 10:00 UTC and (c) 12:00 UTC [14].

Figure 4.7 shows the pressure as function of the time for Schiphol. The pressure is 10 minute average, where 01:00 UTC correspondents to the time slot from 00:50 UTC to 01:00 UTC. The figure shows a linear decrease in the pressure until 09:00 UTC, where a fast increase in the pressure is observed, especially between 10:00 UTC and 12:00 UTC. A small local maximum in the pressure before 09:00 UTC is visible, this can be explained by a shower passing Schiphol at this time.

The KNMI uses 55 weather stations to measure meteorological parameters to determine the weather in the Netherlands and the Dutch part of the North Sea. The 10 m wind from this locations are also used to make plots of the weather in the Netherlands, where figure 4.8 shows the maximal wind gust measured on the 28 of October 2013. It can be seen that the largest wind gusts are measured in the Northern part of the Netherlands, especially above the Wadden Islands. The largest wind gust was measured at Lauwersoog, with wind gusts up to 152 kmh^{-1}.

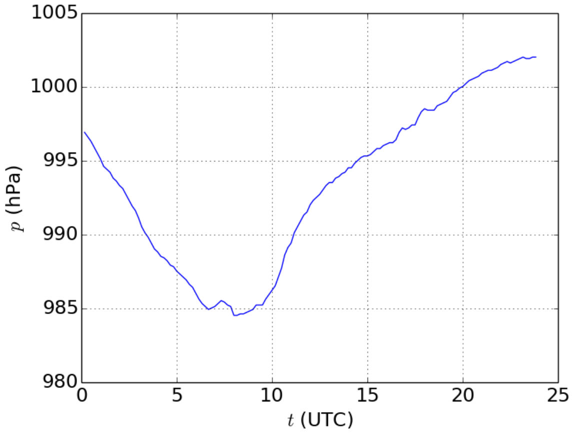

Figure 4.7: The 10 minute average pressure at Schiphol as function of the time.

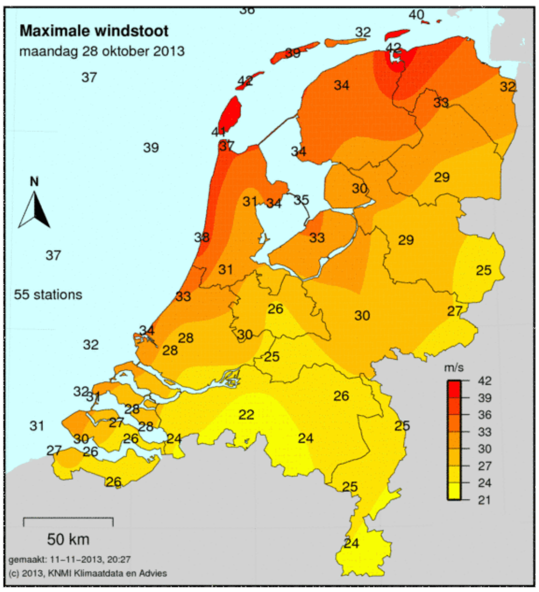

Figure 4.8: The maximal wind gust measured above the Netherlands on the 28 of October 2013.

Aircrafts can be used to determine the wind speed over a wide range of heights in the area around Schiphol. All the aircraft in the area around Schiphol, defined in figure 3.1b, are used to look at the storm of 28 October 2013. A running mean of 10 measurements is used to illustrate the wind speed as function of the time for a height range of 100 m. Figure 4.9 shows the wind speed as function of the time with the standard deviation bars in the time and in the wind speed, with for (a) the aircrafts between 300 and 400 m, and for (b) the aircrafts between 900 and 1000 m.

The wind speed between 300 and 400 m shows a nearly constant value as function of the time until 08:00 UTC. Between 08:00 UTC and 11:00 UTC a jump in the wind speed is visible with 10 ms^{-1} larger values. The wind speed decreases after 11:00 UTC to values around 20 ms^{-1}. At higher altitudes between 900 and 1000 m, the wind speed shows a different pattern than at lower altitudes. The wind speed at this height shows already a high values before the peak of the storm. A small increase in the wind speed from 35 ms^{-1} to 40 ms^{-1} around 10:00 UTC is visible in the wind speed and after 11:00 UTC the wind speed decreases to a wind speed of 25 ms^{-1}. The peak in the wind speed between 09:00 UTC and 11:00 UTC below between 300 and 400 m might be caused by the isallobaric effect. In the lower levels the isallobaric effect could possibly dominate the other components of the ageostrophic wind, where the isallobaric effect might be more counteracted at the higher levels.

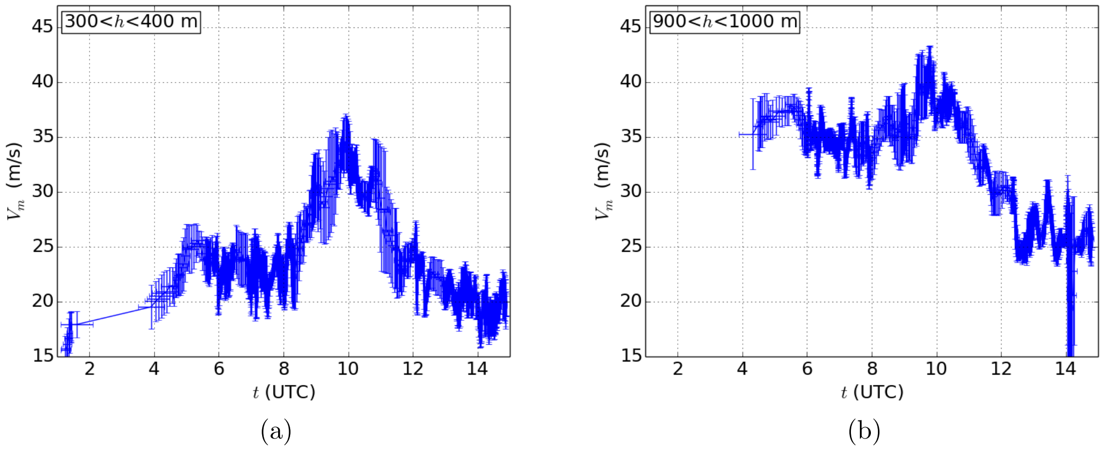

Figure 4.9: The wind speed as function of the time for airplanes in the area around Schiphol, with for (a) between 300 and 400 m and for (b) between 900 and 1000 m.

The most common flight level of the aircrafts is around 10 to 12 km height. The large amount of aircrafts at this flight level range can be used to determine the position of the jet stream, which is mostly situated at heights between 9 and 11 km. The jet stream is situated where cross-front temperature gradient is the large, which is not uniform along the front. Following the thermal wind balance, a local wind maximum will coincide with the most intense part of the front. The acceleration of the air parcels into the jet stream with winds blowing from west to east and the deceleration of the air parcels out of the jet streak will lead to large ageostrophic winds, where the acceleration of the air parcels can be given by [9, page 173-174],

$$\frac{\mathrm{d}u}{\mathrm{d}t} = f v_a. \tag{4.1}$$

The deceleration of the air parcels give that $\frac{\mathrm{d}u}{\mathrm{d}t} < 0$, so that $v_a < 0$, which induces a ageostrophic wind directed towards the higher pressure. Therefore the deceleration set-up a secondary circulation directed perpendicular to the jet streak. The secondary circulation in the exit region of the jet streak induces a downward motion on the warm side of the jet streak and the upward motion on the cold side. The downward motion on the warm side of the jet streak causes a adiabatic temperature increase, and the upward motion of the cold side of the jet streak causes a temperature decrease. Due to the updraft at the left exit region of the jet stream, this region is favorable for the formation of precipitation systems [9, page 173-175].

All aircrafts in the range between 9 and 10 km are used to illustrate the position of the jet stream. Figure 4.10 shows the wind speed from the aircrafts between 09:15 UTC and

09:30 UTC, where the aircraft measurements are interpolated to configure this contour plot. The largest wind speed measured by the Mode-S equipped aircrafts is 81 ms^{-1} observed west of Belgium. This high wind speeds are manifested in the streak, where the exit region of the jet streak is positioned south-west of the Netherlands. This high wind speeds which are observed are also extremely high for winds in the jet stream. The wind speed decreases in the south-east direction too values around 15 ms^{-1} above the Alps.

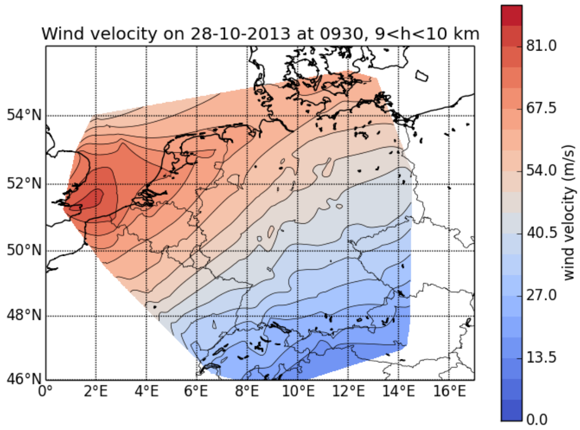

Figure 4.10: The wind velocity at 9 km measured by Mode-S EHS at 09:30 UTC.

Figure 4.11 shows the wind speed between 9 and 10 km and between 11:00 UTC and 11:15 UTC and shows that the position of the jet streak is moved from the previous figure. The jet streak did move in the north-west direction, with the maximum wind speeds above the north-west part of the Netherlands. The left exit region of the jet streak is situated just north the Netherlands, where the center of the cyclone is situated too.

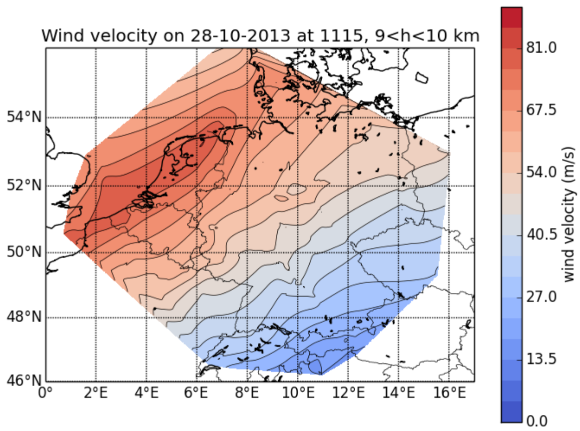

Figure 4.11: The wind velocity at 9 km measured by Mode-S EHS at 11:15 UTC.

The wind speeds around 9.5 km are also shown for a later time between 12:45 UTC and 13:00 UTC in figure 4.12, which shows that the position of the jet streak did not displace from position in comparison with the previous figure. The jet streak did decrease in its intensity to wind speeds between 70 and 80 ms^{-1}. The decrease in intensity in the jet stream also relates to that the cyclone is over its peak intensity in the evolution over time.

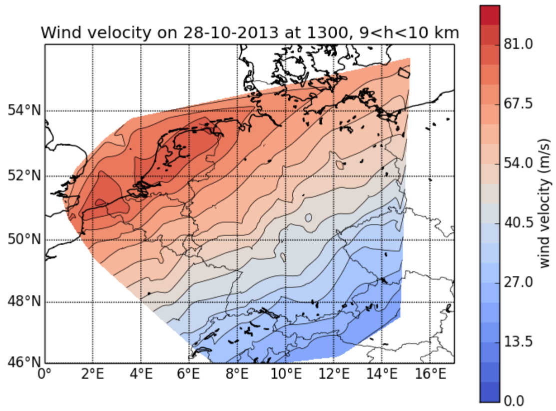

Figure 4.12: The wind velocity at 9 km measured by Mode-S EHS at 13:00 UTC.

The wind as function of the height can be illustrated for the area around Schiphol, where all the aircrafts in a time range of 15 minutes are used to illustrate the wind speed and wind direction as function of the height. Figure 4.13 shows the wind as function of the height for 06:15 UTC, with for (a) the wind speed and for (b) the wind direction. The figure shows a strong increase in the wind speed with height until a pressure of 875 hPa. Then a decrease in the wind speed with as minimum at 800 hPa, and then a further increase in the wind speed with height.

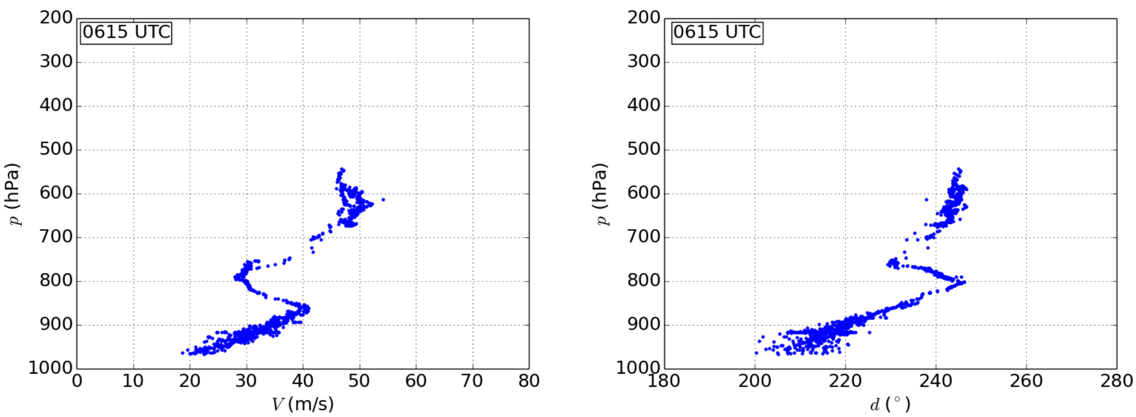

(a) (b)

Figure 4.13: The wind as function of the height for Schiphol at 06:15 UTC, with (a) wind speed and (b) wind direction.

The wind direction as function of the height at 06:15 UTC, shown in sub figure 4.13b, shows a veering of the wind with height until 800 hPa, indicating warm air advection by the geostrophic wind. This is in agreement with the weather maps in figure 4.5a which show a warm front situated in the northern part of the Netherlands [9, page 160-162].

The wind as function of the height is also plotted for 09:15 UTC, shown in figure 4.14 with for (a) the wind speed and for (b) the wind direction. In comparison with the wind at 06:15 UTC, the wind speed is increased and the wind direction becomes nearly constant with the height. A maximum in the wind speed is visible at 700 hPa, where after a small dip, the wind speed increases further with altitude.

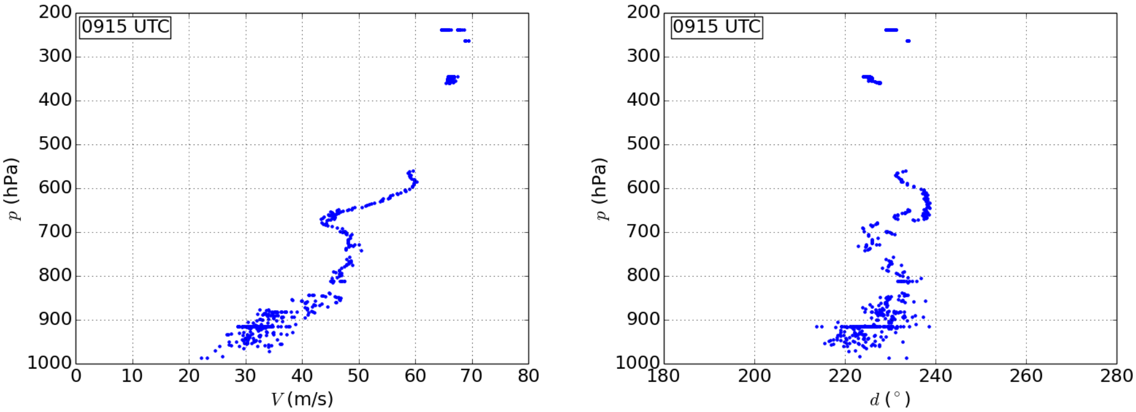

(a) (b)

Figure 4.14: The wind as function of the height for Schiphol at 09:15 UTC, with (a) wind speed and (b) wind direction.

Figure 4.15 shows the wind as function of the height with for (a) the wind speed and for (b) the wind direction. The wind shows a linear increase in the wind speed with altitude, and a veering of the wind with increasing height in the lower 800 hPa of the atmosphere, and a backing of the wind at levels higher than 700 hPa. The backing of the wind with increasing height indicates a cold air advection, which is also in agreement with the cold front that already passed as seen in figure 4.5b.

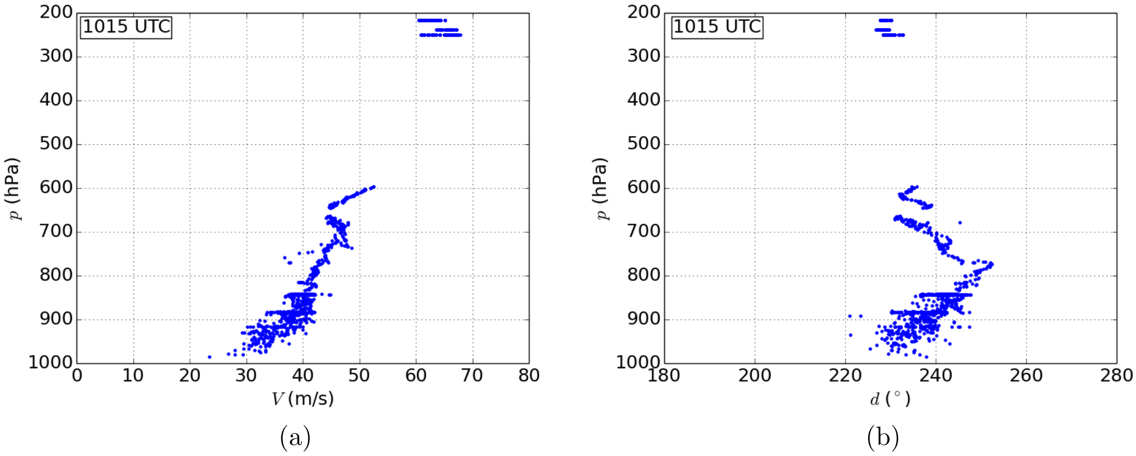

Figure 4.15: The wind as function of the height for Schiphol at 10:15 UTC, with (a) wind speed and (b) wind direction.

4.2 A first step to the theoretical wind

The geostrophic wind and the ageostrophic wind are derived to investigate the cause of the large wind speeds during the storm. These theoretical winds are compared with the wind measured by Mode-S EHS data and the wind from Harmonie version 38. As seen in equation 2.6 and 2.7, the geostrophic wind depends on the change of the height contours in the x- and y-direction on levels of equal pressure. The isallobaric wind can be derived with equation 2.19, where the tendency and the gradient in the height can be calculated in several ways. In this project, two methodologies are used to determine the tendency and the gradient in the height. The height changes on a specific point on a map can be derived by using the finite difference method or the piecewise linear interpolation method. Both methods will be explained before the results of the theoretical wind are discussed.

A rerun of the Harmonie version 38 model of the KNMI has been realized with output for every five minutes between 08:00 UTC and 14:00 UTC. The output used from the Harmonie 38 model are the, u- and v-components of the wind and the geopotential height on a pressure level of 800 hPa. For this case, the model is not initiated with the Mode-S measurements of the wind and the temperature. The Harmonie 38 model is used to determine the height gradient, where the geopotential height is used to determine the height. With the use of the gradient in the height and the wind from the Harmonie 38 model, the theoretical wind is determined for the coordinates of Schiphol.

The theoretical wind is compared with the measured wind speed for Schiphol, where the Mode-S EHS measurements are the mean of the aircraft data in the area around Schiphol in a height range of $\Delta p = \pm 20$ hPa and for the Harmonie 38 model the wind from the gridbox above Schiphol.

4.2.1 Finite difference method

From the gradient of geopotential height the geostrophic wind can be derived. The first method to determine the gradient in the height can be found by using the finite difference method, where the gradient in the height in the x-direction determined from the first order differential around one point, can be written as,

$$\frac{\partial z_{\mathrm{i}}}{\partial x_{\mathrm{i}}} = \frac{z_{\mathrm{i}+1} - z_{\mathrm{i}-1}}{x_{\mathrm{i}+1} - x_{\mathrm{i}-1}}, \tag{4.2}$$

where i is defined as the grid point in the Harmonie 38 model. For the y-direction the same equation holds, which can be written as,

$$\frac{\partial z_{\mathrm{i}}}{\partial y_{\mathrm{i}}} = \frac{z_{\mathrm{i}+1} - z_{\mathrm{i}-1}}{y_{\mathrm{i}+1} - y_{\mathrm{i}-1}}, \tag{4.3}$$

Small variations in the geopotential height between two grid points can have a large contribution to the calculation of the theoretical wind. For this reason the noise in the output of the model takes over the real signal of the gradient in the geopotential height or the wind. It is chosen to increase the distance between the gridpoints from which the theoretical wind is calculated. It is found that a distance of 10 gridpoints is stable to determine the theoretical wind, which also accords with the area around Schiphol. The new first order differential can be written as,

$$\frac{\partial z_{\mathrm{i}}}{\partial x_{\mathrm{i}}} = \frac{z_{\mathrm{i}+10} - z_{\mathrm{i}-10}}{x_{\mathrm{i}+10} - x_{\mathrm{i}-10}} \tag{4.4}$$

$$\frac{\partial z_{\mathrm{i}}}{\partial y_{\mathrm{i}}} = \frac{z_{\mathrm{i}+10} - z_{\mathrm{i}-10}}{y_{\mathrm{i}+10} - y_{\mathrm{i}-10}}. \tag{4.5}$$

The isallobaric wind is defined in equation 2.19. First, the tendency in the geopotential height is determined by the geopotential height at time Φ_t minus the geopotential height at a time step earlier Φ_{t-1}. The time range for the calculation of the isallobaric wind is described in the next sub section. The gradient in the tendency of the geopotential height is then calculated in the same way as the gradient in the height. The geopotential height is divided by the gravitational acceleration to determine the height.

The inertial advective component of the ageostrophic wind is defined in equation 2.21 and 2.22. Both components of the geostrophic wind are determined at the four points which are ten gridpoints apart from the point of interest. From this four points, the inertial advective component can be determined with the use of equation 4.4 and 4.5, where the equation can also be written as function of u_g and v_g. The gradient in the height from which the geostrophic wind at the four points is determined, are calculated in the same way as in equation 4.4 and 4.5. The wind components in equation 2.21 and 2.22 are data collected by the Harmonie 38 model.

4.2.2 Piecewise linear interpolation

[9, page 157-158] Meteorological parameters are measured at several places in the Netherlands. To know, for instance, the wind at a specific location, interpolation can be used to determine the wind speed at that location. A simple method to interpolate the data is by piecewise linear interpolation, where the location has the horizontal coordinates $(x_0,\, y_0)$. This method makes use of three observation points, where the coordinates of this three points are defined as $(x_i,\, y_i)$, with $i = 1, 2, 3$ for the three different locations. The height of a measurement location on a pressure surface can be written as,

$$z_i = z_0 + (x_i - x_0)\frac{\partial z}{\partial x} + (y_i - y_0)\frac{\partial z}{\partial y}, \tag{4.6}$$

where z_0 is the height of the specific location. This equation can be expanded for the three measurement locations, and is written in matrix form as,

$$\begin{pmatrix} z_1 \\ z_2 \\ z_3 \end{pmatrix} = \begin{pmatrix} 1 & (x_1 - x_0) & (y_1 - y_0) \\ 1 & (x_2 - x_0) & (y_2 - y_0) \\ 1 & (x_3 - x_0) & (y_3 - y_0) \end{pmatrix} \begin{pmatrix} z_0 \\ \partial z/\partial x \\ \partial z/\partial y \end{pmatrix}. \tag{4.7}$$

The three unknowns in this equation are z_0, $\partial z/\partial x$, and $\partial z/\partial y$. Equation 4.7 can also be written for other meteorological parameters, just like the wind or temperature. This equation can be simplified to,

$$\begin{pmatrix} z_1 \\ z_2 \\ z_3 \end{pmatrix} = M \begin{pmatrix} z_0 \\ \partial z/\partial x \\ \partial z/\partial y \end{pmatrix}, \tag{4.8}$$

where M is defined as,

$$M = \begin{pmatrix} 1 & (x_1 - x_0) & (y_1 - y_0) \\ 1 & (x_2 - x_0) & (y_2 - y_0) \\ 1 & (x_3 - x_0) & (y_3 - y_0) \end{pmatrix}. \tag{4.9}$$

The simplified form of equation 4.7 can also be written for the unknown parameters as function of the known parameters, which can be written as,

$$\begin{pmatrix} z_0 \\ \partial z/\partial x \\ \partial z/\partial y \end{pmatrix} = M^{-1} \begin{pmatrix} z_1 \\ z_2 \\ z_3 \end{pmatrix}. \tag{4.10}$$

The geostrophic wind is derived from the changes in the height at pressure surfaces in the horizontal direction. The height convergence is calculated from three points around the specific point placed in a triangle, for this thesis written out for Schiphol. A small disturbance in one of the three points in the height measurement can cause an error in the determination of the geostrophic wind. To minimize the chance of an error in the calculated wind speed, the three points in the triangle are turned in steps of ten degrees over the 360 degrees. The determined wind speed is then the mean of the twelve solutions of the wind speed calculated with the piecewise linear interpolation method.

The three points are placed at a specific radius around Schiphol, to be able to investigate this ideal radius, the geostrophic and the isallobaric wind speed are calculated as function of the radius. The isallobaric wind is calculated from the change of the height in time and place, and therefore can be calculated differently for other time steps. With the use of the five minute output of the Harmonie 38 model, the isallobaric wind is calculated with a time range of five, ten and fifteen minutes. The results of the wind as function of the radius for the time range of five and ten minutes are described in appendix B.

Figure 4.16 shows the wind as function of the radius for 10:00 UTC with a time range of dt = ±15 minutes. The sum of the two wind speeds, shown in sub figure 4.16a, shows a fast increase in the wind speed till a radius of 30 km, then a small dip in the wind speed, and then a slightly decrease of the wind speed with increasing radius. The standard deviation in the wind speed increases from 10 to 20 ms^{-1} with increasing radius. The standard deviation in the wind speed and wind direction is described in appendix C.

Sub figure 4.16b shows the wind direction, which is first getting more spacious till 20 km, where after it slightly shrinks with increasing radius. The standard deviation in the wind direction increases from 5 tot 15° with increasing radius.

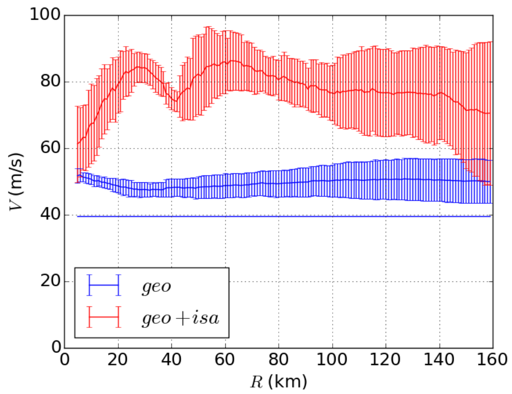

(a)

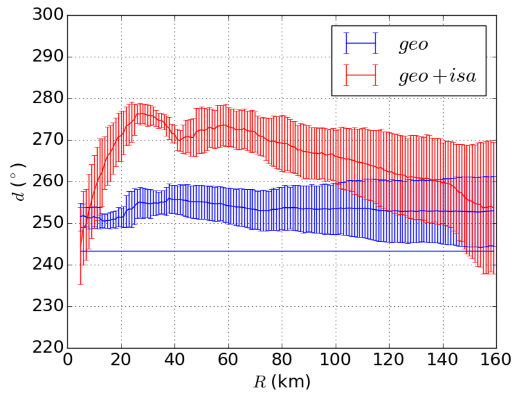

(b)

Figure 4.16: The wind as function of the radius at 800 hPa for 10:00 UTC with for the isallobaric wind a time range of dt = ±15 minutes with for (a) the wind speed and for (b) the wind direction.

The geostrophic wind shows a constant wind speed and wind direction with a radius larger than 20 km. The standard deviation in the wind direction is increasing with a larger radius, so a radius smaller than 60 km has a preference.

The time range of dt = ±5 minutes gives large wind speeds and a large standard deviation. The time ranges of dt = ±10 and dt = ±15 minutes are showing in general the same pattern in comparison with each other, where the time range of dt = ±15 minutes shows a smaller standard deviation than the time range of dt = ±10 minutes. Due to the smaller standard deviation, the time range of dt = ±15 is chosen to determine the isallobaric wind.

From figure 4.16 it can be seen that the wind speed is increasing until 25 km, showing a dip around 40 km, and than increases again. The wind direction get a wider range of directions with increasing radius until 30 km and after 40 km the wind direction gets slightly shrinking. A radius of 35 km is in a range where the wind speed and wind direction are calculated quiet stable. Therefore it is chosen to use a radius of R = 35 km for the derivation of the theoretical wind. As a wrap up, the theoretical wind is determined with a time range of dt = ±15 minutes and a radius of R = 35 km.

4.3 A first result in the theoretical wind

The theoretical wind is determined for the coordinates above Schiphol and compared to the measured wind. Figure 4.17 shows the wind speed as function of the time using the finite difference method at 800 hPa. The wind direction as function of the time is shown in figure 4.18. For both figures the colors of the lines illustrate the same parameter. The black line shows the wind from Harmonie 38, the green line the measured wind by Mode-S EHS, the red line the isallobaric wind, the yellow line the inertial advective wind, the light blue line the total wind, which is defined as the sum of the geostrophic wind plus the ageostrophic wind, and the dark blue line shows the geostrophic wind.

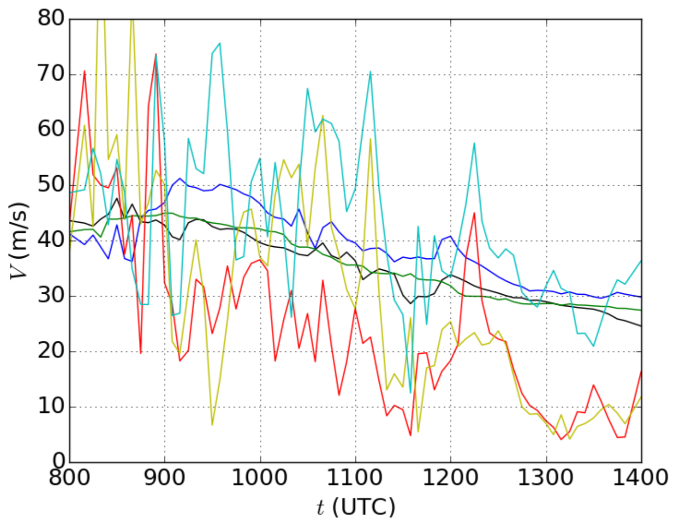

Figure 4.17: The calculated wind speed as function of the time using the finite difference method during the 28 of October 2013 at 800 hPa for, with in black the wind from Harmonie 38, in green the Mode-S wind, in red the isallobaric wind, in yellow the inertial advective wind, in light blue the total wind, and in dark blue the geostrophic wind.

The prediction by Harmonie 38 and the measurements by Mode-S EHS show nearly the same wind speed and wind direction as function of the time, that therefore is in accordance with the results of the comparison discussed in subsection 3.3.4. The geostrophic wind shows a larger wind speed than the wind speed predicted by Harmonie 38 and measured by Mode-S EHS, and also gives a larger wind direction. As stated in section 2.2, the geostrophic wind describes the wind in situations of straight isobars, as result of the curvature of the isobars the wind will decrease in wind speed when the curvature is cyclonic.

The ageostrophic part of the wind, which describes the isallobaric wind and the inertial advective component of the ageostrophic wind, shows a irregular pattern in the wind speed and wind direction as function of the time. This also results in a noisy pattern in the total wind speed during the peak of the storm of the 28 of October 2013 between 08:00 UTC and 11:00 UTC. Before and after the storm, the total wind speed is in the same order as the measured wind speed. The calculated wind direction of the total wind follows the measured wind direction excluding some irregularities.

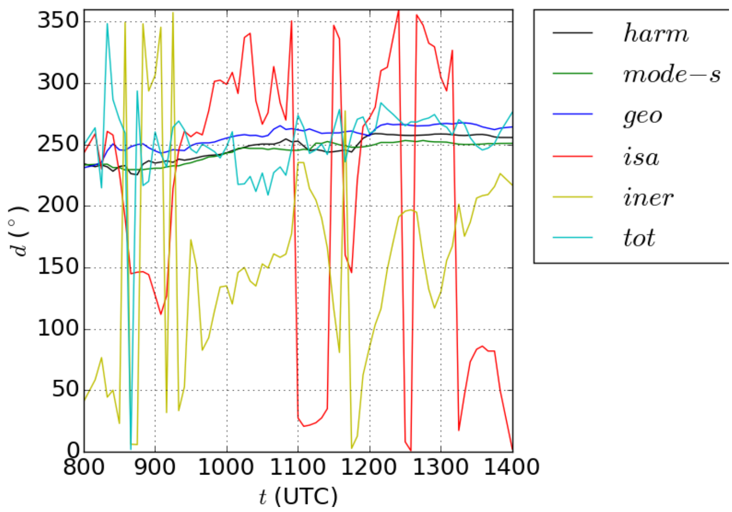

Figure 4.18: The calculated wind direction as function of the time using the finite difference method during the 28 of October 2013 at 800 hPa.

Figure 4.19 shows the wind speed as function of the time using the piecewise linear interpolation method at 800 hPa. Both components of the ageostrophic wind show a noisy pattern in the wind speed, and therefore the total wind speed also shows a irregular pattern as function of the time. But after 13:00 UTC the total wind speed gets in the same order as the measured wind speed.

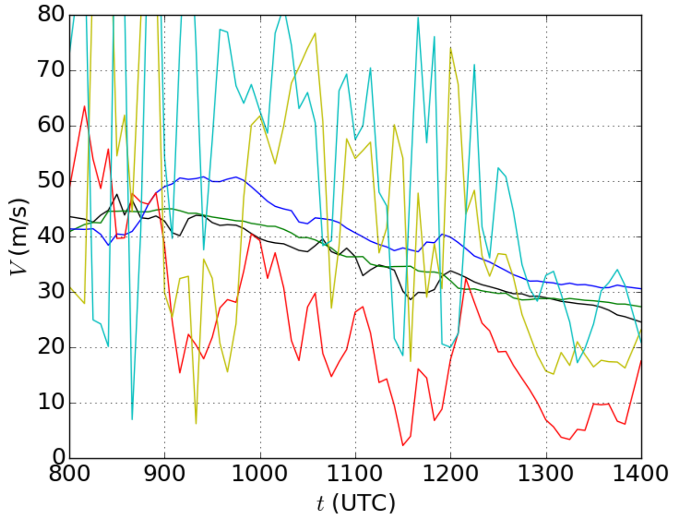

Figure 4.19: The calculated wind speed as function of the time using the piecewise linear interpolation method during the storm of the 28 of October 2013 at 800 hPa.

Figure 4.20 shows the wind direction as function of the time using the piecewise linear interpolation method at 800 hPa. The wind direction of both components of the ageostrophic wind show large irregularities in the solution with time, and therefor also the total theoretical wind direction shows a irregular pattern as function of the time.

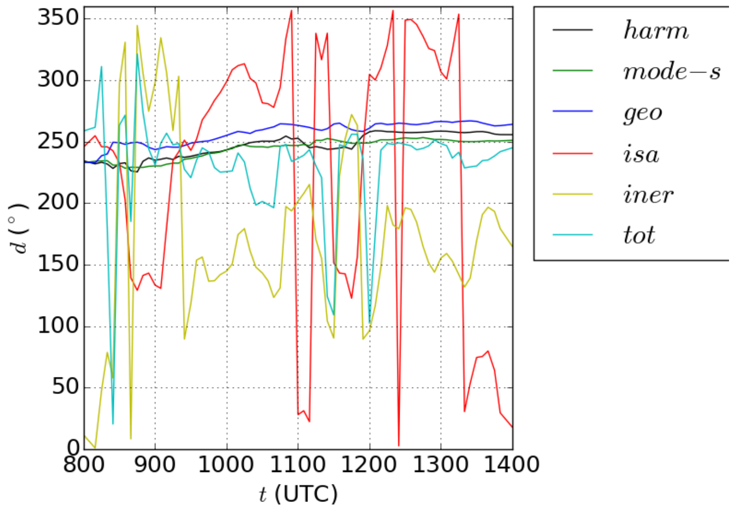

Figure 4.20: The calculated wind direction as function of the time using the piecewise linear interpolation method during the storm of the 28 of October 2013 at 800 hPa.

The geostrophic wind from the finite difference method shows a wind in the same order as the geostrophic wind from the piecewise linear interpolation method. Both methods show large irregularities in the calculations of the total wind. It can be seen that the calculated isallobaric wind from both methods shows the same pattern in the wind speed and wind direction.

4.4 The theoretical wind speed

Due to the large differences between the two methods and the noisy pattern in the total wind seen in section 4.3, it is chosen to expand the original two methods . The geostrophic wind and the inertial-advective component of the wind were calculated at one time step, for example 10:00 UTC, and the isallobaric wind was calculated from 15 minutes before and after 10:00 UTC. Two different time ranges were used to determine the total wind, which should be equal to determine most accurately the wind. Friction with the Earth's surface still plays a role at 800 hPa, so to rather avoid the influences of the surface on the flow in the atmosphere, the calculation of the theoretical wind in this new method are made at a pressure level of 700 hPa.

It is chosen to calculate the geostrophic wind and the inertial advective wind for every five minutes in a time range of thirty minutes, from where the half hour mean theoretical wind is determined from seven calculations. This is done for every five minutes, which results in a running mean of the theoretical wind in time. To get the same set-up for the isallobaric wind, it is chosen to use a time range of $\Delta t = \pm 5$ minutes to determine the isallobaric wind in a time range of 30 minutes. The isallobaric wind is also calculated for every 5 minutes as a running mean over the time.

The theoretical wind from the finite difference method is determined in the same way as discussed in subsection 4.2.1, but for the piecewise linear interpolation method the radius are determined with this new method.

Figure 4.21 shows the wind as function of the radius for 10:00 UTC at 700 hPa, with for (a) the wind speed and for (b) the wind direction. The blue line indicates the geostrophic wind and the red line the sum of the isallobaric wind plus the geostrophic wind. It shows a less noisy result in the sum of the winds than is shown in figure B.1 in subsection 4.2.2. The sum of the two winds shows in the wind speed a nearly constant relation with increasing radius after 30 km, with first a decrease in the wind speed with radius. The wind direction of the sum of the two winds shows first a veering of the wind with radius, where after 60 km the wind backs with increasing radius. The radius of 35 km, chosen in section 4.2, is in the wind speed the transition from decrease to a small increase in the wind speed, where this radius in the wind direction is in the border from veering of the wind to backing of the wind. It is chosen to set the radius of this new method also to 35 km, which shows a stable solution for the calculation of the geostrophic wind and the isallobaric wind.

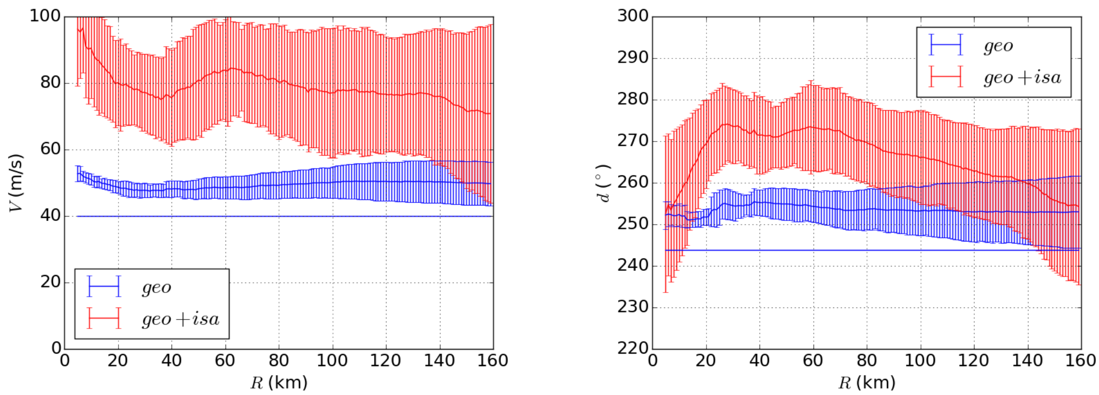

(a) (b)

Figure 4.21: The wind as function of the radius at 700 hPa for 10:00 UTC shown as a running mean of 30 minutes with for the isallobaric wind a time range of dt = ±5 minutes with for (a) the wind speed and for (b) the wind direction.

The theoretical wind is compared with the measured and predicted wind speed for Schiphol in the same way as described in section 4.2 for both methods. In the next section, the wind during the storm is also illustrated on a map over the Netherlands, where the distribution of the different wind components is shown.

4.5 Results of the theoretical wind

The theoretical wind is derived for grid points over the Netherlands for 10:00 UTC and at the location of Schiphol as function of the time, where the winds are now calculated as half hour mean winds following section 4.4. Figure 4.22 shows the geostrophic wind vectors on a map with on the background the half hour mean of the geopotential height (m^2s^{-2}) on 700 hPa at 10:00 UTC from Harmonie 38, with for (a) the piecewise linear interpolation method and for (b) the finite difference method. The geostrophic wind for both methods shows a wind speed which is the largest near the line of $\Phi = 27000\,m^2s^{-2}$, where the lines of equal geopotential height are also the closest to each other. It also shows that the geostrophic wind at this time is the strongest in the northern part of the Netherlands. The geostrophic wind determined from both methods shows the same wind speed and wind direction, with some small differences at specific grid points.

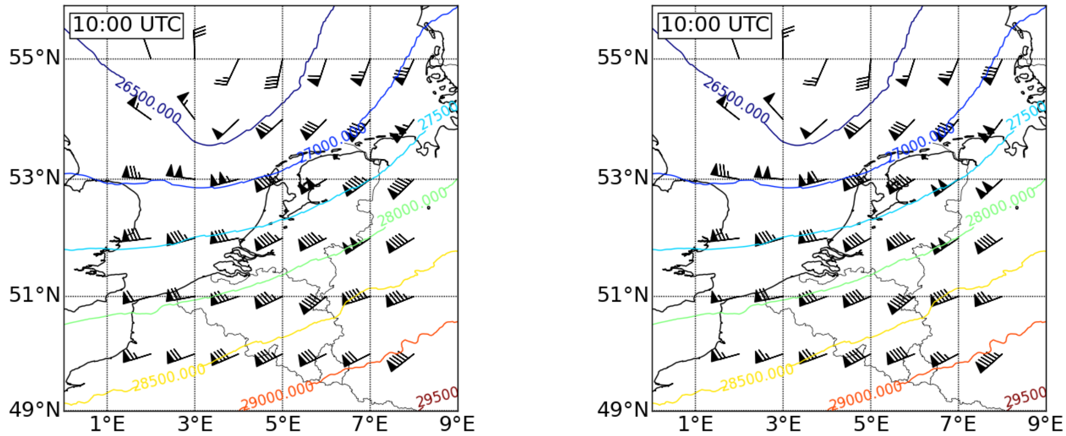

(a) (b)

Figure 4.22: The geostrophic wind vector on 700 hPa at 10:00 UTC with for (a) the piecewise interpolation method and for (b) the finite difference method. The barbs, which are attached to the wind vectors which point in the direction where the wind comes from, indicates the wind speed. Each barb corresponds to 5 ms^{-1}, each half barb to 2.5 ms^{-1} and each triangle to 25 ms^{-1}.

Figure 4.23 shows the isallobaric wind vector with on the background the tendency in the geopotential height on 700 hPa at 10:00 UTC from the Harmonie 38 model, with for (a) the piecewise linear interpolation method and for (b) the finite difference method. The tendency in the geopotential height is determined from the geopotential height at 10:15 UTC minus the geopotential height at 09:45 UTC divided by the number of seconds in half an hour. The yellow and orange colors indicate areas of pressure rises while the blue colors indicate areas of pressure falls. The areas of pressure falls in larger and less intense than the area of pressure increases, which covers a relative small area with strong pressure increases. It can be seen that the isallobaric wind is pointed down the gradient of pressure tendencies, for instance from areas of pressure rises to areas of pressure falls. The isallobaric wind is the strongest in areas of large pressure tendencies, and therefore in agreement with the theory described in section 2.2. The strength of the calculated isallobaric wind in this area is in the order of 175 ms^{-1}, but is not observed in the atmosphere at these altitudes.

The tendency in the geopotential height shows an area of small pressure rises at the east border of the Netherlands that is due to the rain front in this region, which can also be seen from the cold air front in figure 4.5b. This front introduces some stronger isallobaric winds. The isallobaric wind determined for both methods shows in general the same wind speed and wind direction, with some small differences between the two.

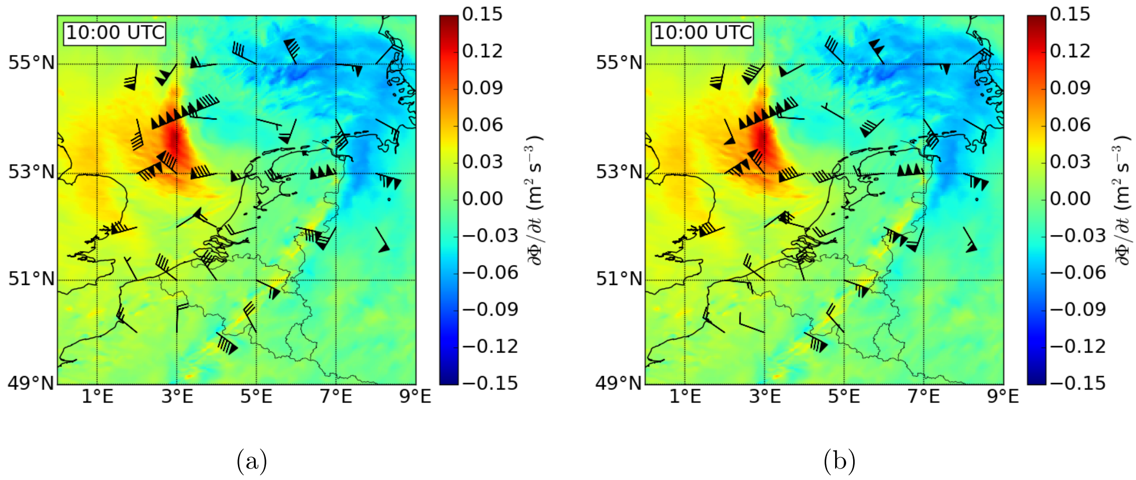

Figure 4.23: The isallobaric wind vector on 700 hPa at 10:00 UTC with for (a) the piecewise interpolation method and for (b) the finite difference method.

Figure 4.24 shows the inertial advective component of the ageostrophic wind vector with on the background the geopotential height (m^2s^{-2}) on 700 hPa at 10:00 UTC from Harmonie 38, with for (a) the piecewise linear interpolation method and for (b) the finite difference method. The wind shows in areas just south of the center of the cyclone winds in opposite direction as the geostrophic wind, and therefore is in agreement with the theory described in section 2.2. The rest of the Netherlands shows a inertial advective wind that is directed to the northwest. Near the front, situated at the east border of the Netherlands, the inertial advective wind is pointed away from the front.

The inertial advective component of the ageostrophic wind derived by the two methods, shows some differences, where the wind speed determined from the finite difference method is higher than the wind speed determined from the piecewise linear interpolation method. The wind direction shows large similarities between the two near the center of the cyclone, but south of 51° N, the wind direction is different for both methods. The inertial advective component of the wind is determined from two differentials, first the gradient in the height and second the gradient in the geostrophic wind. The double differential, small irregularities in the geopotential height result in large calculated wind speeds. The piecewise linear interpolation shows a result from the mean of twelf calculations per time step, where the finite difference method uses one calculation per time step. Like observed in the result, the inertial advective wind calculated from the piecewise linear interpolation method is lower than the wind calculated from the finite difference method.

Figure 4.25 shows the ageostrophic wind as function of the time using the finite differ-

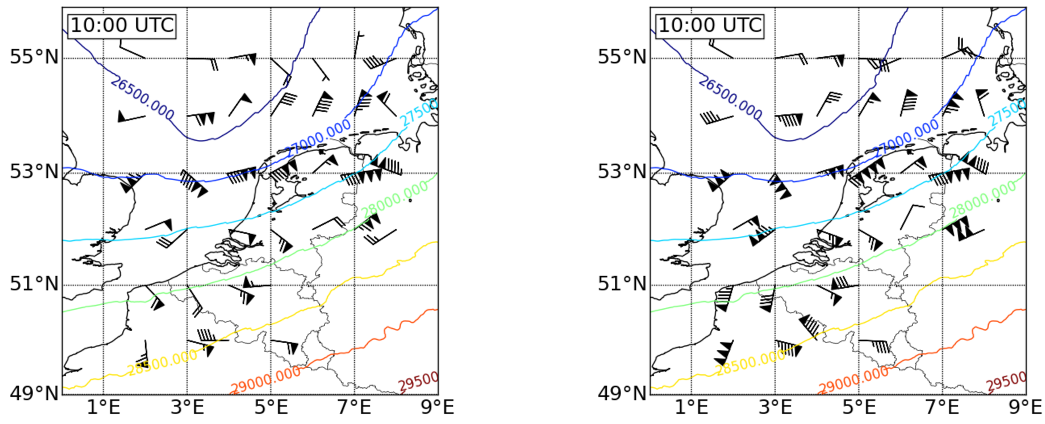

(a)

(b)

Figure 4.24: The inertial advective component of the ageostrophic wind vector on 700 hPa at 10:00 UTC with for (a) the piecewise interpolation method and for (b) the finite difference method.

ence method at 700 hPa, with for (a) the wind speed and for (b) the wind direction. The ageostrophic wind from this method shows a less noisy pattern than the first method did, demonstrated in figure 4.17, that therefore is the result of averaging over 30 minutes. From figure 4.25a it can be seen that wind speed of both components of the ageostrophic wind follows the same pattern in time, where the inertial advective component of the wind is a bit higher. The ageostrophic wind direction, illustrated in figure 4.25b, shows that the isallobaric wind and the inertial advective component of the wind are directed in opposite direction of each other.

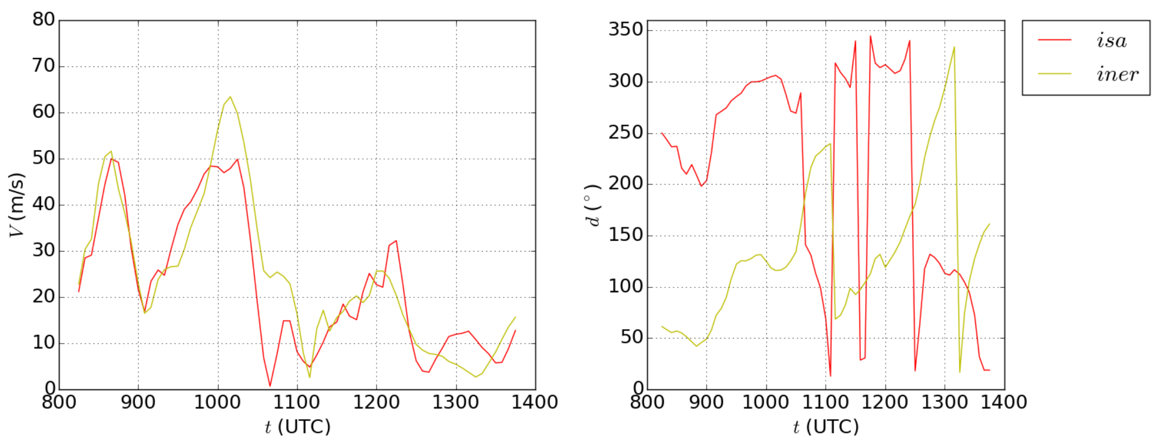

(a)

(b)

Figure 4.25: The calculated ageostrophic wind as function of the time, using the finite difference interpolation method during the 28 of October 2013 at 700 hPa for (a) the wind speed and for (b) the wind direction.

Figure 4.26 shows the wind as function of the time using the finite difference method at 700 hPa, with for (a) the wind speed and for (b) the wind direction. The colors of the lines are configured in the same way as explained in section 4.3. The Mode-S EHS and Harmonie 38 measure nearly the same wind speed and wind direction over the time, where the Mode-S EHS measures higher wind speeds around 10:00 UTC than the predicted wind speed by Harmonie 38. The geostrophic wind shows a wind speed in the same order as the measured wind, with a higher wind speed calculated between 08:00 UTC and 10:00 UTC. The geostrophic wind direction is calculated larger than the measured wind direction, this can be explained by the curvature of the isobars.

The total wind varies with a range of 15 ms^{-1} around the measured and geostrophic wind, which also follows from the fact that both components of the ageostrophic wind counteract each other. Due to this fact, the total wind direction varies around the measured wind direction, where the total wind direction is also calculated more spacious than the measured wind around 11:00 UTC.

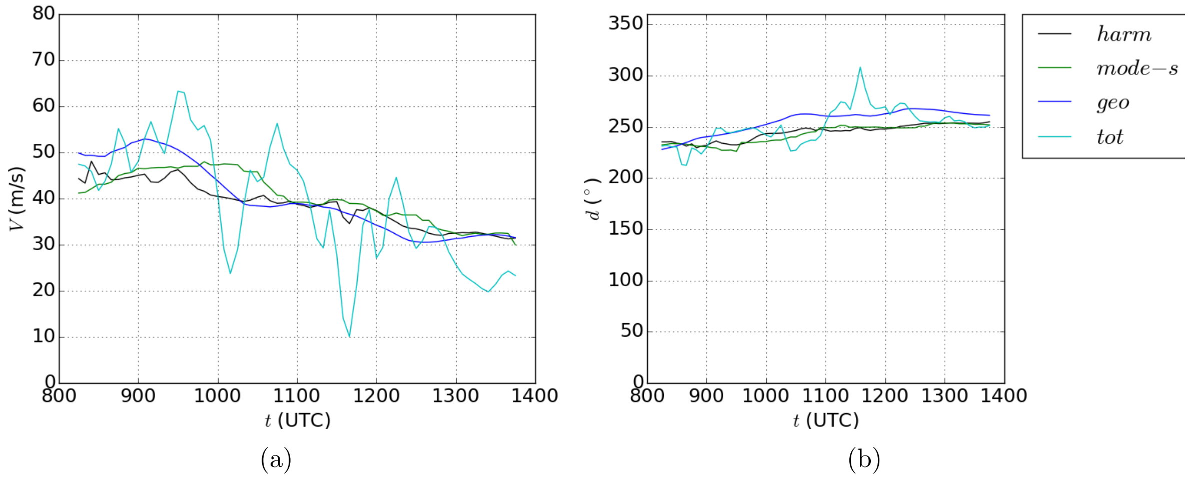

Figure 4.26: The calculated wind as function of the time, using the finite difference interpolation method during the 28 of October 2013 at 700 hPa for (a) the wind speed and for (b) the wind direction.

Figure 4.27 shows the ageostrophic wind as function of the time using the piecewise linear interpolation method at 700 hPa, with for (a) the wind speed and for (b) the wind direction. The isallobaric wind is determined in te same order as the geostrophic wind as function of the time, except from 09:00 UTC to 10:00 UTC and after 12:00 UTC, where the isallobaric wind is determined lower. The inertial advective wind shows a large wind speed from 10:00 UTC to 12:00 UTC, with even wind speeds up to 70-80 ms^{-1}. But as seen from the wind direction, between 08:00 UTC and 09:00 UTC and between 11:00 and 12:00 UTC, both components of the ageostrophic wind are directed in opposite direction of each other.

Figure 4.28 shows the wind as function of the time using the piecewise linear interpolation method at 700 hPa, with for (a) the wind speed and for (b) the wind direction. The components of the ageostrophic wind show the same pattern in the wind speed in time, but the wind speed is different. The inertial advective wind shows in general a larger wind speed than the isallobaric wind, except from 09:00 UTC to 09:30 UTC.

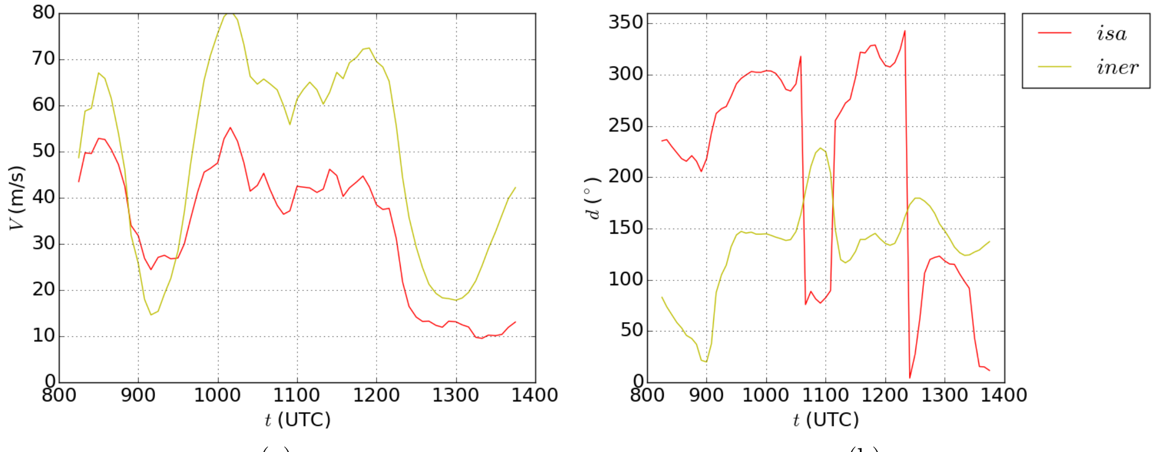

Figure 4.27: The calculated ageostrophic wind as function of the time using the piecewise linear interpolation method during the 28 of October 2013 at 700 hPa for (a) the wind speed and for (b) the wind direction.

This results in a total wind speed which is large between 09:00 UTC and 11:00 UTC with wind speeds up to 60-70 ms^{-1} and a wind speed which follows the measured wind speed the rest of the time. The total wind direction is calculated smaller than the measured wind direction.

The large peak in the calculation of the total wind between 09:00 UTC and 11:00 UTC also corresponds with the same pattern measured in the lower atmosphere as shown in figure 4.9a. The three components of the wind can be used to determine the possible wind speeds that are measured near the earth surface. It is not enough to use only the isallobaric wind to describe the measured wind speed, due to the fact that the inertial advective wind also counteracts the isallobaric wind.

The differences in the theoretical wind between the two methods are still visible, where the total wind from the finite difference method shows a more noisy signal than the total wind from the piecewise linear interpolation method. This is the result of the large varying wind direction of both components of the ageostrophic wind with the finite difference method. The pattern in the total wind from the piecewise linear interpolation method corresponds with the pattern measured in the lower atmosphere, so this method is scientifically more accurate than the finite difference method.

Figure 4.29 shows the total wind vector with on the background the geopotential height (m^2s^{-2}) on 700 hPa at 10:00 UTC from Harmonie 38, with for (a) the piecewise linear interpolation method and for (b) the finite difference method. The black barbs indicate the calculated total wind and the blue barbs indicate the wind from Harmonie 38, which is the wind from the gridbox at the location of the barb. It explains that the total wind from the finite difference method deviates more from the modelled wind than the total wind from the piecewise linear interpolation method. The finite difference method also calculates higher wind speeds for the total wind than from the model.

Looking to the general view of the wind in figure 4.29a the calculated total wind follows the wind from Harmonie 38, except for some irregularities in the calculated wind. The total

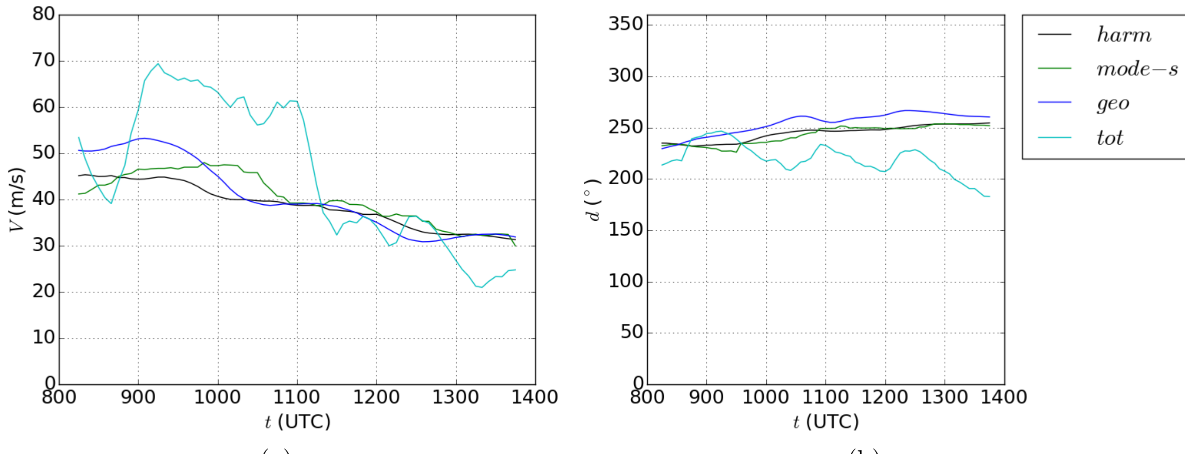

Figure 4.28: The calculated wind as function of the time using the piecewise linear interpolation method during the 28 of October 2013 at 700 hPa for (a) the wind speed and for (b) the wind direction.

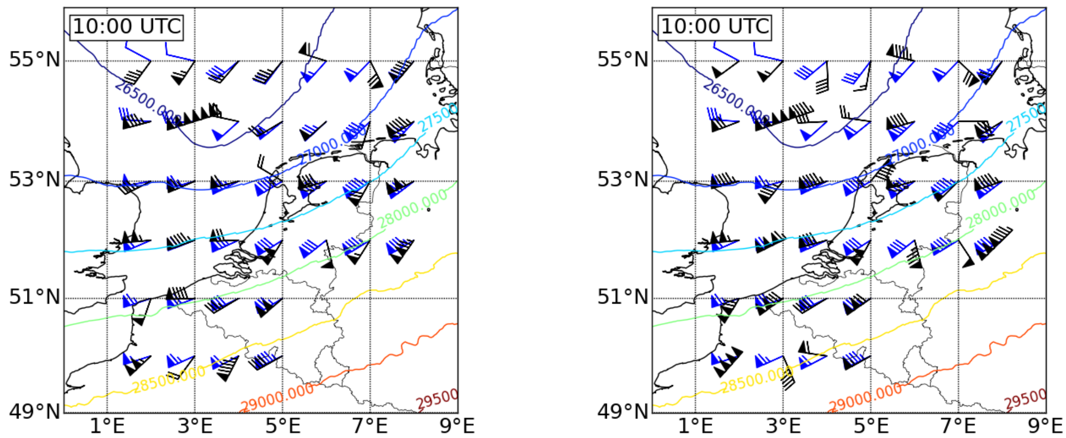

Figure 4.29: The total wind vector on 700 hPa at 10:00 UTC with in blue the wind from Harmonie 38 and in black the calculated total theoretical wind vector with for (a) the piecewise interpolation method and for (b) the finite difference method.

wind is calculated quiet high in the trough, which is due to the large calculated isallobaric wind. Some barbs show deviations from the model which is due to the large inertial advective wind. The wind near the east border also deviates from the model, which is due to the warm front, which induces larger ageostrophic wind.

The wind by Mode-S is measured in a wide range of heights in the area around Schiphol, which is not fully used to illustrate the wind during the storm. All the aircraft measurements during this day are used to illustrate the wind as function of the height and as function of the time in a contour plot. A time range of 10 minutes and a height range of 75 m are used to illustrate this. If a height and time range does not include aircraft measurements, this gap in the contour plot is then interpolated from the measurements of the surrounding boxes.

Figure 4.30 shows the contour plot of the wind speed by Mode-S EHS as function of the height and the time, where the red colors indicate large wind speeds, and blue colors indicate low wind speeds. In the lower 800 m of the atmosphere the wind speed is around 20 - 25 ms^{-1} before and after the storm, but during the peak of the storm between 09:00 UTC and 11:00 UTC the wind speed increases to 30 - 35 ms^{-1}. At altitudes higher than 800 m the wind speed is already 35 - 40 ms^{-1} before of the storm and increases slightly during the peak of the storm to 40 - 50 ms^{-1}, where the wind speed decreases fast after the storm to 25 - 30 ms^{-1}. The strong peak in the wind speed in the lower 800 m of the atmosphere can be caused by isallobaric effect which dominates the other components of the ageostrophic wind.

As also seen in previous figures the inertial advective component of the ageostrophic wind counteracts the isallobaric wind in the higher atmosphere around 3 km. Figure 4.30 shows that the wind speed behaves in the same pattern at altitudes higher than 800 m. This indicates that the isallobaric wind is counteracted by the inertial advective component of the ageostrophic wind in the atmosphere higher than 800 m.

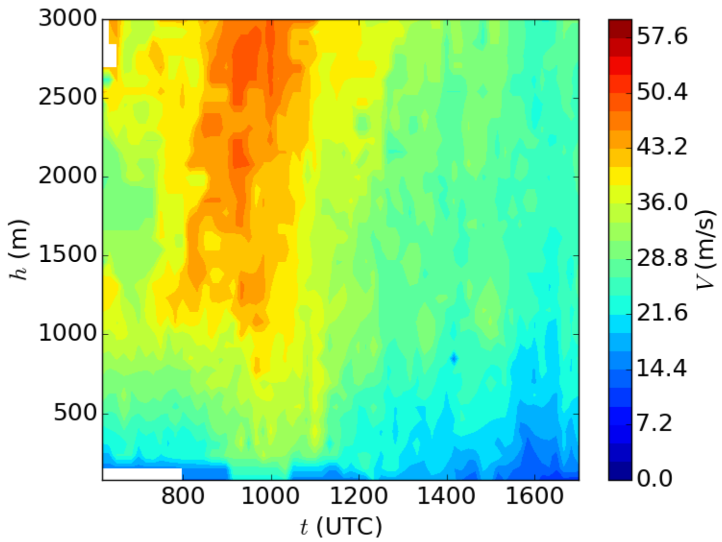

Figure 4.30: The wind velocity by Mode-S EHS as function of the height and the time for the area around Schiphol.

Figure 4.31 shows the contour plot of the wind speed by Harmonie 36 as function of the height and the time. The same settings as figure 4.30 as chosen. The instant model output of 9 vertical levels per hour are used in this contour plot. The Harmonie model shows that the wind speed between 700 m and 2000 m shows a peak in the wind speed, where the increase in wind speed near the surface is less than measured. The pressure level of 1000 hPa is also used in this contour plot that is below mean sea level during a part of the day. The wind speed at levels higher than 2000 m are also high before the peak of the storm.

The harmonie 36 model shows some differences in the wind speed with the Mode-S EHS measurements. Near the surface the Mode-S EHS measures nearly the same wind speed as the Harmonie 36, where the lowest level of Harmonie 36 most not be taken into account. But at higher altitudes than 2000 m, there is a large difference in the wind speed measured by Mode-S EHS and expected by Harmonie 36. The model gives larger wind speeds than Mode-S EHS, mostly in the upper 2500 m of the contour plot. It should be taken into account that one hour model output is used, and that a factor of three less vertical levels are used for the model in comparison with Mode-S EHS. But in general, the wind speed by Mode-S EHS compares well with the expected wind speed by Harmonie 36, even in conditions of a severe storm.

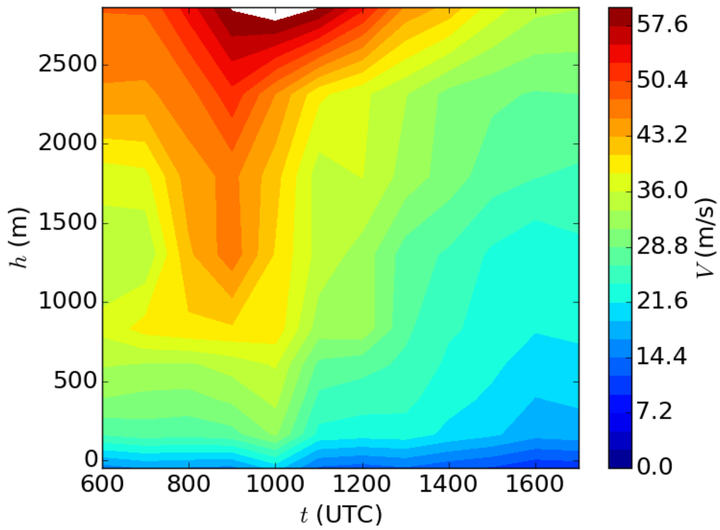

Figure 4.31: The wind velocity by Harmonie 36 as function of the height and the time for the grid box nearest to Schiphol.

Chapter 5

Discussion and conclusion

Aircrafts can be used to derive upper air wind and temperature information, which is used in the case study in the storm of the 28 of October 2013. The quality of the Mode-S EHS data is validated by a comparison with the Cabauw tower, the wind profiler and the Harmonie 36 model. The three measuring systems show a correlation with each other within 4 % and a maximal standard deviation of $\sigma = 2\,\mathrm{ms}^{-1}$ in the wind speed, and for the wind direction with $2\,^{\circ}$ and a maximal standard deviation of $\sigma = 14\,^{\circ}$. The differences between the three measuring systems can be caused by the large distance of 39 km between Schiphol and Cabauw, where the three measuring methods also cause some differences between the systems.

The comparison of the Mode-S EHS with the Harmonie 36 model shows a 3 % smaller wind speed by Mode-S with a standard deviation of $3\,\mathrm{ms}^{-1}$ and an equal wind direction within a standard deviation of $5\,^{\circ}$. The wind by Harmonie 36 is an instant value of the wind speed and wind direction, the Mode-S EHS is an average of minimal five measurements that results in a lower wind speed measured by Mode-S EHS.

The isallobaric wind has a large contribution to the total wind speed, especially in regions near the center of a cyclone, where the gradient in the pressure tendencies is large. The inertial advective component of the ageostrophic wind is directed in opposite direction to the geostrophic wind, mainly in the area just south of the cyclone.

The total wind speed is in agreement with the measured wind speed outside the peak of the storm, but during the peak of the storm the total theoretical wind speed is calculated $20\,\mathrm{ms}^{-1}$ larger than the measured wind speed. This peak in the derived total wind speed illustrated the ageostrophic component of the wind which is not observed at 700 hPa, but what is observed in the lower 800 m of the atmosphere. So the combination of both components of the ageostrophic wind could be the source of the peak in the wind speed near the surface as seen in the observations.

The Mode-S EHS data is a new measurement technique to derive wind information from a tracking radar of the air traffic control. This data is of good quality shown in the comparison with the wind profiler, the KNMI Cabauw Tower and the Harmonie model version 36 and 38. Even in situations of a severe storm, the comparisons between the Mode-S EHS and both versions of the Harmonie model are good. This indicated that the Mode-S EHS is of good quality and has an extremely large data set of measurements in a wide range of altitudes in the atmosphere.

From the observations by the Mode-S EHS it can be concluded that the isallobaric wind has no component in the total wind at 700 hPa. In the lower 800 m of the atmosphere the isallobaric wind could possibly dominate the other components of the ageostrophic wind, and could be possibly the source of the high wind speeds measured during this severe storm. But it can not concluded that the isallobaric effect is the source of the strong wind speeds measured in the lower 800 m of the atmosphere during this severe storm.

Chapter 6

Outlook

The Mode-S EHS data is compared with the KNMI tower and the wind profiler at Cabauw situated 39 km away from Schiphol. The Mode-S EHS could be compared with the SODAR (SOnic Detection And Ranging), which measures the wind as function of the height until 700 m and situated at Schiphol, to drop the large distance between Schiphol and Cabauw.

The results show that the strong wind speed where a manifest in the lowest 800 m of the atmosphere. It therefore is of interest to determine the theoretical wind at 950 hPa from the geopotential height from Harmonie 38. The contour plot of the wind speed by Harmonie 36 as function of the time and the height is plotted with 1 hour model output. With the rerun of the Harmonie 38 model per 5 minutes, the contour plot can be made with a higher time resolution, but only 4 levels where available at the time of writing this thesis. With the model output for every 5 minutes, the Mode-S EHS data could be better compared with the model data.

Some aircrafts are equipped with ADS-B software which is developed to extract meteorological information from the aircrafts. The position of the aircrafts by Mode-S EHS is determined by the radar, where by ADS-B this is determined by the GPS (Global positioning system) in the aircrafts. The ADS-B data also contains the geometric height of the aircraft, besides the pressure level of the aircraft. With the use of several aircrafts on the same pressure level, the geostrophic and isallobaric wind can be derived from the height of the aircraft with the use of the piecewise linear interpolation method.

Bibliography

[1] De Haan, S. (2013). An improved correction method for high quality wind and temperature observations derived from Mode-S EHS. *KNMI publication: TR-338.*

[2] de Haan, S., and Stoffelen, A. (2009). High resolution temperature and wind observations from commercial aircraft. *In Proceedings of the 8th International Symposium on Tropospheric Profiling.*

[3] De Haan, S. (2011). High?resolution wind and temperature observations from aircraft tracked by Mode?S air traffic control radar. *Journal of Geophysical Research: Atmospheres, 116*(D10).

[4] Holton, J. R., and Hakim, G. J. (2012). *An introduction to dynamic meteorology* (Vol. 88). Academic press.

[5] Nagelkerke, N. J. (1991). A note on a general definition of the coefficient of determination. *Biometrika*, 78(3), 691-692.

[6] Rochette, S. M., and Market, P. S. (2006). A primer on the ageostrophic wind. *Natl. Weather Dig*, 30, 17-28.

[7] Van Den Hoog, H. (2014). Rekenen aan de wind op 28 oktober 2013. *Meteorologica*, 25-2, 20-24

[8] Van Delden, A. (2013). Stormen verwachten kunnen we goed maar hoe moeten we windhozen zien aankomen. *Meteorologica*, 24-4, 4-8

[9] Van Delden, A. (2014). *Atmospheric Dynamics.*

[10] Vaisala wind profiler, LAP 3000 (2005). 1st ed. *Vaisala.*

[11] https://en.wikipedia.org/wiki/St._Jude_storm (16-05-2016)

[12] http://bhw432.knmi.nl/ tijm/minmax_obs/Rankfc_cl.txt (04-07-2016)

[13] https://www.wunderground.com/blog/weatherhistorian/most-powerful-storm-in-14-years-sweeps-northwestern-europe (25-05-2016)

[14] http://www.buienradar.nl/nederland/neerslag/buienradar-terugkijken/archief/201310281100 (25-06-2016)

[15] http://www.eumetrain.org/eport/view.php?width=1366&height=768&date=2013102806&region=euro (07-08-2016)

Appendix A

List of abbreviations and units

Table A.1: The abbreviations used in this thesis

Abbreviation	Definition
ADS-B	Automatic Dependent Surveillance-Broadcast
ECMWF	European Centre for Medium-Range Weather Forecasts
$iner$	inertial advective component of the ageostrophic wind
ICAO	International Civil Aviation Organization
isa	isallobaric wind
geo	geostrophic wind
$harm$	wind from the harmonie model
KNMI	Royal Dutch Meteorological Institute
Mode-S EHS	Mode Secondary Enhanced Surveillance
$mode-s$	wind from Mode-S
tot	total wind

Table A.2: The symbols used in this thesis with its units

Symbol	Definition	Unit
ϕ	latitude	$^\circ$
λ	longitude	$^\circ$
Ω	angular velocity of the earth	s^{-1}
Γ	atmospheric lapse rate	Km^{-1}
Δ	bias	-
σ	standard deviation	-
Φ	geopotential height	$\mathrm{m}^2\mathrm{s}^{-2}$
ρ	density	kgm^{-3}

Table A.3: The symbols used in this thesis with its units

Symbol	Definition	Unit
a	radius of the earth	m
d	direction	$^\circ$
f	Coriolis parameter	s^{-1}
F	flight level of an aircraft	m
F_{rx}	horizontal frictional forces	ms^{-2}
F_{ry}	horizontal frictional forces	ms^{-2}
g	gravitational acceleration	ms^{-2}
h_{cor}	correction height of aircrafts	m
$\hat{k}$	unit vector in the vertical direction	-
$\hat{i}$	unit vector in the x-direction	-
$\hat{j}$	unit vector in the y-direction	-
m	Mach number	-
M	Matrix	-
n	number of measurements	-
p	pressure	hPa
p_0	pressure at sea level	hPa
p_1	pressure-altitude of an aircraft	hPa
R^2	correlation coefficient	-
R_d	gas constant of dry air	$J \times kg^{-1}K^{-1}$
t	time	s
T	temperature	K
T_0	standard temperature at sea level	K
u	x-component of the horizontal wind speed	ms^{-1}
u_g	x-component of the geostrophic wind speed	ms^{-1}
u_{iner}	x-component of the inertial advective wind	ms^{-1}
v	y-component of the horizontal wind speed	ms^{-1}
v_a	y-component of the ageostrophic wind	ms^{-1}
v_g	y-component of the geostrophic wind speed	ms^{-1}
v_{iner}	y-component of the inertial advective wind	ms^{-1}
$\vec{V}$	total wind vector	ms^{-1}
$\vec{V_a}$	ageostrophic wind vector	ms^{-1}
$\vec{V_g}$	geostrophic wind vector	ms^{-1}
$\vec{V_{isa}}$	isallobaric wind vector	ms^{-1}
$\vec{V_{gr}}$	Ground speed vector of an aircraft	ms^{-1}
$\vec{V_t}$	True airpeed vector of an aircraft	ms^{-1}
w	vertical wind speed	ms^{-1}
x	distance in longitudinal direction	m
y	distance in latitudinal direction	m
z	vertical direction	m

Appendix B

Radius determination

This chapter discusses the technical information of the isallobaric wind as function of the radius for a time range of five and ten minutes.

Figure B.1 shows the geostrophic wind and the sum of the geostrophic wind plus the isallobaric wind, as function of the radius of the triangle for 10:00 UTC and the time range of $\mathrm{d}t = \pm 5$ minutes. Sub figure B.1a shows the wind speed as function of the radius and sub figure B.1b shows the wind direction as function of the radius. The blue line with barbs in both the figures shows the geostrophic wind, the red line with barbs shows the sum of the two winds and the straight blue line shows the wind from the Harmonie 38 model at the grid box closest to Schiphol. The geostrophic wind shows a nearly constant calculated wind speed and direction, where the standard deviation is small but increases slightly while the radius increases.

The sum of the geostrophic and isallobaric wind shows a large standard deviation, both in the wind speed as in the wind direction, with increasing standard deviation as function of the radius. The summation in the wind speed is larger over the whole radius range than the wind speed modelled by Harmonie 38. In the first 20 km, the wind speed is even calculated larger than 100 ms^{-1}. The calculated wind direction shrinks with increasing radius, that gets closer to the wind direction by Harmonie 38.

Figure B.2 shows the geostrophic wind and the sum of the geostrophic wind with the isallobaric wind as function of the radius for 10:00 UTC with a time range of $\mathrm{d}t = \pm 10$ minutes. The geostrophic wind and the wind from the Harmonie 38 model are the same as in figure B.1, because of their in-dependency in the length of the time range. The summation of the geostrophic wind plus the isallobaric wind shows a slight increase in the wind speed up to 30 to 40 km, with from then a small decrease in the calculated wind speed. The standard deviation in the wind speed varies from 15 to 20 ms^{-1}, which is increasing with larger radius.

The sum of the winds is strongly getting more spacious with increasing radius till 20 km, with after it slightly shrinks with increasing radius. The standard deviation in the wind direction is increasing from 5 to 15° with increasing radius.

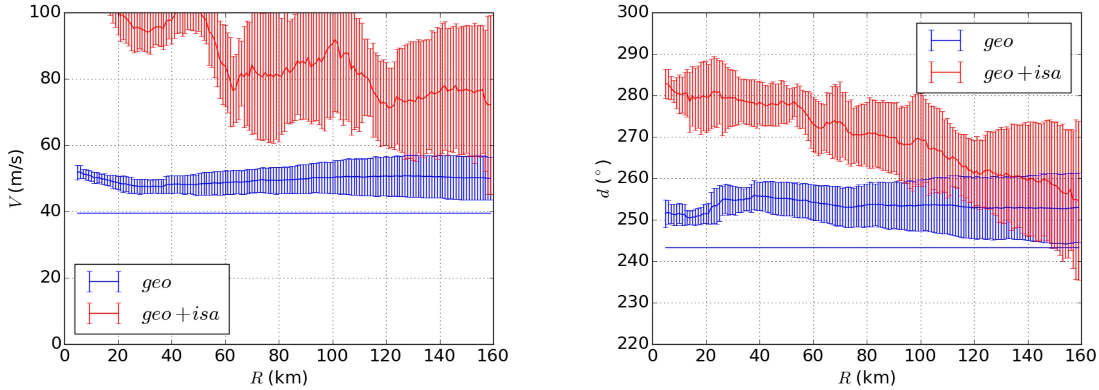

(a) (b)

Figure B.1: The wind as function of the radius at 800 hPa for 10:00 UTC with for the isallobaric wind a time range of d$t = \pm 5$ minutes with for (a) the wind speed and for (b) the wind direction. The wind shown with error bars, with in blue the geostrophic wind and in red the sum of the geostrophic wind plus the isallobaric wind.

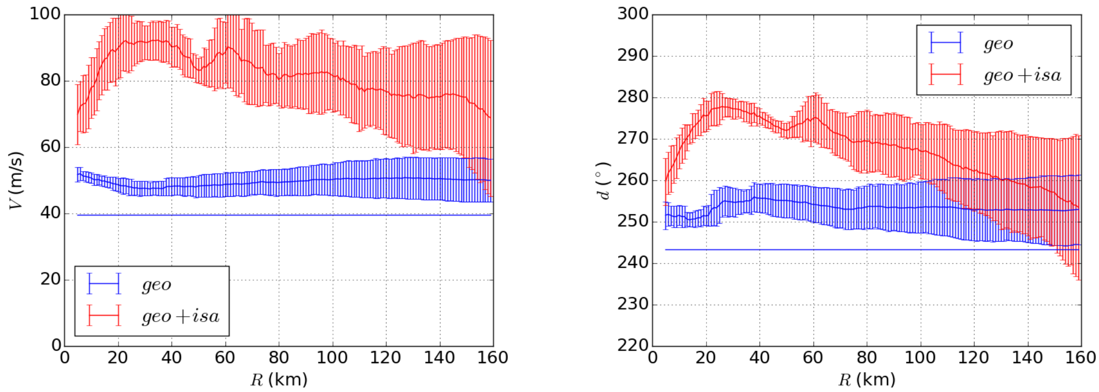

(a) (b)

Figure B.2: The wind as function of the radius at 800 hPa for 10:00 UTC, with for the isallobaric wind a time range of d$t = \pm 10$ minutes with for (a) the wind speed and for (b) the wind direction.

Appendix C

Standard deviation in the wind

The standard deviation in the wind speed can be determined by derivative of the function over the two components of the wind speed times the variation in the components of the wind speed, which can be written as,

$$\Delta V = \left|\frac{\partial V}{\partial u}\right| \Delta u + \left|\frac{\partial V}{\partial v}\right| \Delta v, \tag{C.1}$$

where Δu indicates the standard deviation in the u-component of the wind speed and Δv indicates the standard deviation in the v-component of the wind speed. The standard deviation in the total wind speed is then written out as,

$$\Delta V = \left|\frac{u}{\sqrt{u^2+v^2}}\right| \Delta u + \left|\frac{v}{\sqrt{u^2+v^2}}\right| \Delta v. \tag{C.2}$$

The standard deviation in the wind direction can be written as,

$$\Delta d = \left|\frac{\partial d}{\partial u}\right| \Delta u + \left|\frac{\partial d}{\partial v}\right| \Delta v, \tag{C.3}$$

where this can be written out with the derivatives to,

$$\Delta d = \left|\frac{v}{u^2+v^2}\right| \frac{180}{\pi} \Delta u + \left|\frac{u}{u^2+v^2}\right| \frac{180}{\pi} \Delta v \tag{C.4}$$

Appendix D

Pressure

The flight level of the aircraft is corrected for the approximation of a pressure of 1013.25 at sea level, where the flight level is corrected for the difference in the measured surface pressure and the approximated pressure at sea level. From the hydrostatic balance follows,

$$\frac{\mathrm{d}p}{\mathrm{d}z} = -\rho g, \tag{D.1}$$

where p is the pressure in Pa, z is height above sea level in m, ρ is the density in kgm^{-3} and g is the gravitational acceleration. From the equation of state, the density can be written as,

$$\rho = \frac{p}{RT}, \tag{D.2}$$

where R is the specific gas constant of fry air ($R = 287$ Jkg^{-1}K^{-1}) and T is the temperature in K. With the equation of state, the hydrostatic balance can be written as,

$$\frac{1}{p}\mathrm{d}p = -\frac{g}{RT}\mathrm{d}z. \tag{D.3}$$

The temperature is assumed to decrease with height, which is defined by the lapse rate of the atmosphere,

$$\gamma = -\frac{\mathrm{d}T}{\mathrm{d}z}, \tag{D.4}$$

where $\gamma = 0.0065$ Km^{-1}. With integration the temperature at a specific height can be written as,

$$T = T_0 - \gamma z, \tag{D.5}$$

where T_0 is the temperature at sea-level which is assumed to be 288.15 K??. Substituting this equation into integral of equation D.3 results in,

$$\int_{p_0}^{p_1} \frac{1}{p}\mathrm{d}p = -\frac{g}{R}\int_0^z \frac{1}{T_0 - \gamma z}\mathrm{d}z, \tag{D.6}$$

where p_0 is the pressure at sea level and p_1 is the pressure at a specific height. Integrating over the boundaries results in,

$$\ln(p_1) - \ln(p_0) = \frac{g}{\gamma R} \left(\ln(T_0 - \gamma z) - \ln(T_0) \right), \tag{D.7}$$

which can be also be written as,

$$\ln\left(\frac{p_1}{p_0}\right) = \frac{g}{\gamma R} \ln\left(\frac{T_0 - \gamma z}{T_0}\right), \tag{D.8}$$

where the sea level pressure is assumed to be $p_0 = 101325$ Pa, $g = 9.81$ ms^{-12} and where p_1 is the pressure measured by the Schiphol weather station. The equation can be written as,

$$\mathrm{e}^{\frac{\gamma R}{g} \ln\left(\frac{p_1}{p_0}\right)} = \left(\frac{T_0 - \gamma z}{T_0}\right). \tag{D.9}$$

The correction height can be written as,

$$h_{corr} = -\frac{T_0}{\gamma} \left(\left(\frac{p_1}{p_0}\right)^{\left(\frac{\gamma R}{g}\right)} - 1 \right). \tag{D.10}$$

The real height of the airplane is determined by,

$$h = h_p + h_{corr}, \tag{D.11}$$

where h_p is the flight level in m with the assumption of constant sea level pressure.